

## RESEARCH ARTICLE

# PTEX helps efficiently traffic haemoglobinases to the food vacuole in *Plasmodium falciparum*

Thorey K. Jonsdottir<sup>1,2<sup>✉</sup>a<sup>b</sup>\*</sup>, Brendan Elsworth<sup>1<sup>✉</sup>c</sup>, Simon Cobbold<sup>3<sup>✉</sup>d</sup>, Mikha Gabriela<sup>1,4<sup>✉</sup>e</sup>, Ellen Ploeger<sup>1</sup>, Molly Parkyn Schneider<sup>1</sup>, Sarah C. Charnaud<sup>1<sup>✉</sup>f</sup>, Madeline G. Dans<sup>1<sup>✉</sup>e</sup>, Malcolm McConville<sup>3</sup>, Hayley E. Bullen<sup>1,2<sup>✉</sup>g</sup>, Brendan S. Crabb<sup>1,2,5<sup>✉</sup>g</sup>, Paul R. Gilson<sup>1,2<sup>✉</sup>g</sup>

1 Malaria Virulence and Drug Discovery Group, Burnet Institute, Melbourne, Australia, 2 Department of Immunology and Microbiology, University of Melbourne, Melbourne, Australia, 3 Department of Biochemistry and Molecular Biology, Bio21 Institute of Molecular Science and Biotechnology, University of Melbourne, Melbourne, Australia, 4 School of Medicine, Deakin University, Geelong, Australia, 5 Department of Immunology and Pathology, Monash University, Melbourne, Australia



## OPEN ACCESS

**Citation:** Jonsdottir TK, Elsworth B, Cobbold S, Gabriela M, Ploeger E, Parkyn Schneider M, et al. (2023) PTEX helps efficiently traffic haemoglobinases to the food vacuole in *Plasmodium falciparum*. PLoS Pathog 19(7): e1011006. <https://doi.org/10.1371/journal.ppat.1011006>

**Editor:** Ron Dzikowski, Hebrew University, ISRAEL

**Received:** November 14, 2022

**Accepted:** July 16, 2023

**Published:** July 31, 2023

**Copyright:** © 2023 Jonsdottir et al. This is an open access article distributed under the terms of the [Creative Commons Attribution License](#), which permits unrestricted use, distribution, and reproduction in any medium, provided the original author and source are credited.

**Data Availability Statement:** All relevant data are within the manuscript and its [Supporting Information](#) files.

**Funding:** This work was supported by the National Health and Medical Research Council (NHMRC) grant numbers: 1092789, 1128198 and 119780521 awarded to BSC. The funders had no role in study design, data collection and analysis, decision to publish, or preparation of the manuscript.

✉ These authors contributed equally to this work.

<sup>a</sup> Current address: Department of Molecular Biology, Umeå University, Umeå, Sweden

<sup>b</sup> Current address: The Laboratory for Molecular Infection Medicine Sweden (MIMS), Umeå, Sweden

<sup>c</sup> Current address: Division of Emerging and Transfusion Transmitted Diseases, Office of Blood Research and Review, Center for Biologics Evaluation and Research, Food and Drug Administration, Silver Spring, Maryland, United States of America

<sup>d</sup> Current address: Ubiquitin Signalling Division, Walter and Eliza Hall Institute, Melbourne, Australia

<sup>e</sup> Current address: Infectious Diseases and Immune Defences Division, Walter and Eliza Hall Institute, Melbourne, Australia

<sup>f</sup> Current address: Research for Health Department, World Health Organization, Geneva, Switzerland

\* [thorey.jonsdottir@umu.se](mailto:thorey.jonsdottir@umu.se); [paul.gilson@burnet.edu.au](mailto:paul.gilson@burnet.edu.au)

## Abstract

A key element of *Plasmodium* biology and pathogenesis is the trafficking of ~10% of the parasite proteome into the host red blood cell (RBC) it infects. To cross the parasite-encasing parasitophorous vacuole membrane, exported proteins utilise a channel-forming protein complex termed the *Plasmodium* translocon of exported proteins (PTEX). PTEX is obligatory for parasite survival, both *in vitro* and *in vivo*, suggesting that at least some exported proteins have essential metabolic functions. However, to date only one essential PTEX-dependent process, the new permeability pathways, has been described. To identify other essential PTEX-dependant proteins/processes, we conditionally knocked down the expression of one of its core components, PTEX150, and examined which pathways were affected. Surprisingly, the food vacuole mediated process of haemoglobin (Hb) digestion was substantially perturbed by PTEX150 knockdown. Using a range of transgenic parasite lines and approaches, we show that two major Hb proteases; falcipain 2a and plasmepsin II, interact with PTEX core components, implicating the translocon in the trafficking of Hb proteases. We propose a model where these proteases are translocated into the PV via PTEX in order to reach the cytostome, located at the parasite periphery, prior to food vacuole entry. This work offers a second mechanistic explanation for why PTEX function is essential for growth of the parasite within its host RBC.

**Competing interests:** The authors have declared that no competing interests exist.

## Author summary

*Plasmodium falciparum* is the causative agent of the most severe form of malaria in humans, where the symptoms of the disease are derived from the continuous asexual replication of the parasite within the human red blood cells (RBCs) it infects. To survive within this niche, the parasite exports hundreds of parasite effector proteins across the vacuole it resides within and into the RBC. About a quarter of the exported proteins appear to be essential during the blood stage but the functions of these proteins largely remain uncharacterised. Protein export is facilitated by an essential protein complex termed the *Plasmodium* translocon of exported proteins (PTEX). Conditional depletion of PTEX's core components results in rapid parasite death presumably because essential proteins do not reach their functional destination in the RBC and their associated metabolic functions cannot be performed. To uncover what these essential metabolic functions are we knocked down a core component of PTEX, PTEX150, using a previously established conditional knockdown parasite line. Metabolic analysis of the knockdown parasites indicated that haemoglobin (Hb) digestion was inhibited resulting in a reduction of Hb derived peptides, which serve as an amino acid source for the parasite. We determined that knocking down HSP101, another PTEX core component, also disrupted the Hb digestion pathway. Furthermore, we provide evidence that reduction of Hb digestion might be due to the failure to efficiently deliver early acting Hb digesting proteases to the cytostome, a specialised location where vesicles of Hb are taken into the parasite. PTEX may therefore play a role in delivering Hb proteases to the cytostome.

## Introduction

Malaria is a disease caused by *Plasmodium* parasites and transmitted to humans with the bite of an infected female *Anopheles* mosquito. Malaria remains a major health and economic burden and it is estimated that 619,000 people died of malaria in 2021 [1]. The clinical symptoms of malaria are derived from the asexual replicative stage of the parasite, which occurs within the red blood cells (RBCs) the parasite infects [2]. During this stage the parasite invades the RBC and resides within a parasitophorous vacuole (PV); a membranous sac serving to occlude the parasite away from the RBC cytosol. The intracellular parasite is thus encased in two membranes, the parasite plasma membrane (PPM) and the parasitophorous vacuole membrane (PVM) [3]. For survival within the infected RBC (iRBC), the parasite employs its own ATP-powered protein conduit at the PVM termed the *Plasmodium* translocon of exported proteins (PTEX) to export parasite effector proteins across the PVM and into the iRBC to establish essential host cell modifications [4–7].

PTEX is a 1.6 MDa complex comprising three core proteins: Exported protein 2 (EXP2), PTEX150 and heat shock protein 101 (HSP101). Within this complex, EXP2 exists as a heptamer, which forms the PVM pore and binds directly to PTEX150, a heptamer that serves as a structural connector between EXP2 and HSP101. HSP101 exists as a hexamer and unfolds proteins prior to delivery through PTEX150 for transit through EXP2 and into the iRBC [4,8–11]. These three components cannot be knocked out in the human malaria parasite *P. falciparum* or the rodent malaria parasite *P. berghei* and conditional knockdown results in rapid parasite death and a block in protein export across the PVM, indicating PTEX mediated export is essential for parasite survival [4–7,11–13].

Bioinformatic analyses have helped predict which proteins are likely exported based on the presence of a pentameric motif on their N-terminus called the *Plasmodium* export element

(PEXEL) motif and other export related features [14–18]. Some exported proteins, however, lack the PEXEL motif, and are referred to as PEXEL negative exported proteins (PNEPs). Since PNEPs lack a signature export motif it is harder to predict their export [19]. It is hypothesised that ~25% of the predicted exported proteome (exportome) is essential for *in vitro* blood stage growth but the essential functions remain unclear [20,21]. To date, only one essential function has been assigned to exported proteins, the establishment of the new permeability pathways (NPPs) at the iRBC surface, which help import essential nutrients from the surrounding blood plasma [22–27]. However, most exported proteins that have annotated functions are not essential for *in vitro* growth and contribute to iRBC rigidity, virulence and immune evasion [28–30].

Here we conditionally knocked down one of PTEX's core components, PTEX150, (using the previously established PTEX150-HA $glmS$  parasite line [6]) and used metabolomics to identify biological processes affected when PTEX's function is perturbed and thereby the potential function(s) of the essential exportome. Metabolomic data revealed a potential link between haemoglobin (Hb) digestion and PTEX function. To strengthen this finding, we also observed an association of two major Hb proteases, falcipain 2a (FP2a) and plasmepsin II (PM II) with PTEX. Overall, the data provided in this study suggests that PTEX core components help with efficient trafficking of Hb proteases within the PV space *en route* to the food vacuole where Hb digestion occurs.

## Results

### Conditional knockdown of PTEX150 reduces the level of digested Hb

To perturb the function of one of PTEX's principal components, we used a previously established PTEX150-HA $glmS$  parasite line [6], where PTEX150 had been appended with a triple haemagglutinin (HA) protein tag and a  $glmS$  riboswitch to conditionally knockdown PTEX150 in the presence of glucosamine (GlcN) [31]. Metabolomic analyses were performed on 18, 24 and 30-h post invasion (hpi) parasites synchronised to a 4 h window, one cell cycle after the addition of 0.15 mM or 1 mM GlcN to induce knockdown of PTEX150-HA expression (Figs 1A, S1A and S2).

Analysis of resultant data revealed that various metabolites, such as those involved in glycolysis and nucleotide metabolism were perturbed in PTEX150-HA $glmS$  knockdown parasites, indicating cellular homeostasis was dysregulated (S1 Table). This was predominantly observed in parasites 30-hpi, a treatment time at which the PTEX150-HA $glmS$  knockdown parasites are known to stall [6] which was also evident by Giemsa-stained smears in this study (S2 Fig). These effects are therefore most likely a result of parasite growth arrest rather than a direct involvement of PTEX in these pathways (S1 Table and S1A Fig).

The data also revealed that PTEX150-HA knockdown resulted in a noticeably lower abundance of Hb peptides when compared to untreated samples, indicating that Hb digestion was reduced in these parasites (Figs 1A and S1A and S1 Table). The largest difference in Hb peptide abundance was observed at 24-hpi and 30-hpi in parasites treated with 1 mM GlcN (Fig 1A). However, unlike for other metabolites, this effect was also observed in parasites treated with 0.15 mM GlcN, which does not significantly affect parasite growth (Figs 1A and S1A) as evident by Giemsa-stained smears (S2 Fig) and previously published work [6]. Therefore, reduction of digested Hb is likely due to PTEX150-HA knockdown and not due to a defect in overall parasite growth. In further support of this, a moderate decrease in certain Hb peptides was also observed at 18-hpi and a noticeable decrease in 24-hpi parasites treated with either 0.15 or 1 mM GlcN (Fig 1A), no growth delay is observed at 18-hpi by Giemsa-stained smears

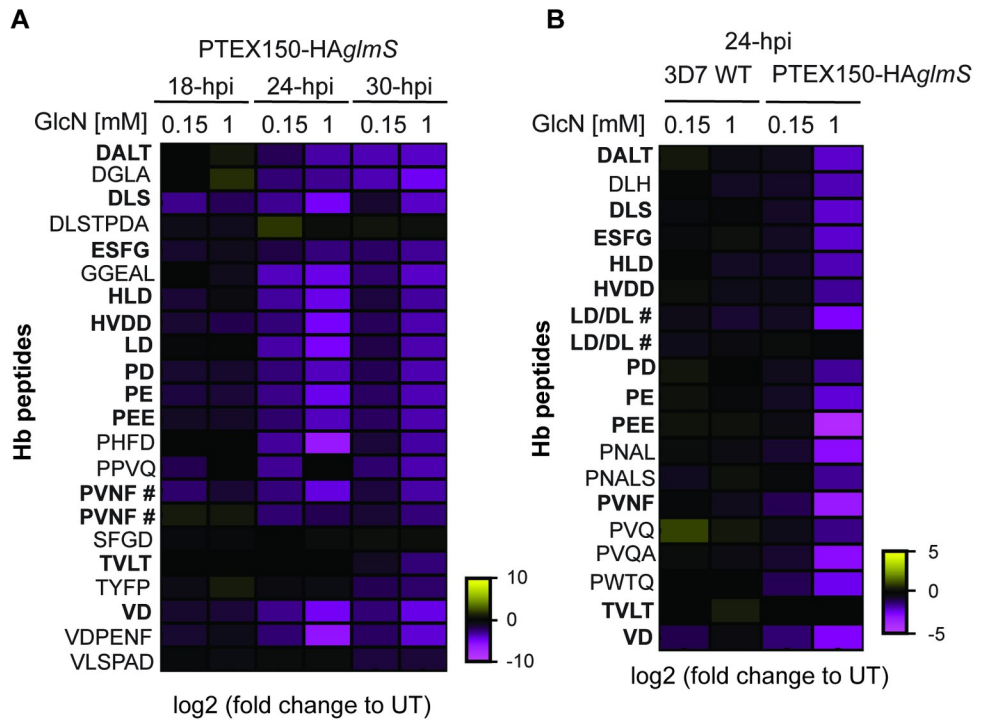


**Fig 1. Conditional knockdown of PTEX150-HAglmS perturbs the Hb digestion pathway.** (A) Highly synchronous PTEX150-HAglmS trophozoite stage parasites were treated with 0, 0.15 or 1 mM GlcN for one cell cycle to knockdown the expression of PTEX150-HA. The parasites were harvested at 18, 24 and 30-hpi and their metabolites were extracted and fractionated for identification by mass spectrometry. The fold change for 0.15 and 1 mM GlcN compared to untreated (UT) parasites is indicated. The amino acid sequences of the Hb peptides are shown on the left of the heat map. Heat map shows 1 biological replicate completed in technical triplicate. # PVNF was identified as one continuous peak with two apexes and therefore treated as two independent peaks. (B) Metabolites from 3D7 WT and PTEX150-HAglmS parasite lines were prepared as described for panel A and parasites harvested at 24-hpi. The heat map represents 1 biological replicate of 3 technical replicates, where fold change is shown for 0.15 or 1 mM GlcN compared to untreated. Fold change for both heat maps was calculated using the following formula =  $\log_2$  (GlcN treated / untreated). In bold are peptides that are shared between panel A and B. # The instrument cannot discriminate between the two sequences, LD and DL, and therefore it has a duplicate entry as LD/DL.

<https://doi.org/10.1371/journal.ppat.1011006.g001>

or at 24-hpi during 0.15 mM GlcN treatment (S2 Fig). Overall, these data indicate that knockdown of PTEX150-HA might perturb Hb digestion.

To corroborate these findings, the experiment was repeated using a single time point and a 3D7 wild-type (WT) parasite control to monitor any effects caused by the GlcN treatment itself on Hb peptide abundance. The parasites were synchronised and GlcN-treated as for previous metabolomics assay using a single time point (24-hpi). This time point was chosen because the majority of Hb digestion occurs 18–32-hpi and we start to see a dramatic decrease in Hb digestive peptides at this stage when PTEX150-HA is knocked down (Fig 1A) [32,33]. As previously observed, the most dramatic metabolic differences between the lines following PTEX150-HA knockdown are in the levels of Hb peptides (Figs 1B and S1B and S1 Table). Specifically, the 3D7 WT parasites showed a slight decrease in some Hb peptides when treated with GlcN, but the reduction observed for PTEX150-HAglmS expressing parasites was much greater (Figs 1 and S1). No growth delay was observed for 3D7 WT parasites when treated with GlcN (S2 Fig). Collectively from these data we hypothesised that PTEX might have a role in the Hb digestion pathway.

## Establishing a falcipain 2a knockdown line as a positive control for disturbance to Hb digestion

It was not immediately obvious how knockdown of PTEX reduces Hb peptides and so we postulated that PTEX could either be involved in the uptake of Hb or involved in the trafficking of the early acting falcipain and plasmepsin Hb proteases to the cytostome *en route* to the food vacuole / digestive vacuole [34–36]. These Hb proteases show a certain level of redundancy where knocking out one protease can sometimes be rescued by another protease, but not all of them can be knocked out simultaneously (extensively reviewed in [37]). The cytostome is an invagination of both the PPM and the PVM from which Hb containing vesicles bud off for transport to the food vacuole where the majority of Hb digestion occurs [38,39]. Uptake of Hb and digestion are both important for parasite survival, providing both amino acids (aa) and space for the growing parasite. The parasite consumes more Hb than needed for aa synthesis and it is hypothesised that this helps maintain the osmotic stability of the iRBC [33,40–43]. Falcipain 2a (FP2a) is one of the early acting Hb proteases [44–46] and due to this, it was chosen for this study to determine if knocking down FP2a expression would mimic the effects observed for PTEX150-HAglmS knockdown. We appended the C-terminus of the *fp2a* gene (PF3D7\_1115700) with a single HA-tag and the *glmS* riboswitch using the CRISPR/Cas9 approach (S3A Fig). C-terminal tagging has not previously been found to affect FP2a trafficking or function [34–36]. Furthermore, FP2a is not individually essential for *in vitro* growth [47,48], therefore knocking it down would not be expected to severely reduce parasite growth.

Correct integration of the tag to the *fp2a* locus was confirmed via PCR (S3B Fig) and western blot was used to confirm the presence of FP2a-HA, where both pro- (54 kDa) and mature (27 kDa) forms of the protease were observed as has been reported previously [45,49] (S3C Fig). To investigate the level of knockdown, FP2a-HAglmS trophozoite stage parasites were treated with increasing concentrations of GlcN for one cell cycle and >90% protein knockdown was observed by western blot (S3C Fig). Immunofluorescence assays (IFAs) were then used to determine the localisation of FP2a-HA within the iRBC where it showed diffuse localisation in the parasite cytoplasm (S3D Fig), often with concentrated puncta around the parasite surface, possibly representing the cytostome as has been previously observed [34,36,50] (S3D Fig, white arrows). While green fluorescent protein (GFP) tagged FP2a is shown to concentrate in the food vacuole, FP2a-HA was found throughout the parasite cytoplasm as previously observed with a native FP2a antibody [34]. This is not entirely unexpected, as previous reports of a HA-tagged food vacuole protein, lipocalin (PF3D7\_0925900), showed that the HA-tag is degraded upon food vacuole entry [51]. The HA-tag of our FP2a-HA could therefore also be degraded and not easily detectable inside the food vacuole by IFA. However, we did observe the processed form of FP2a-HA by western blot, which could indicate that in its non-reduced form used for IFA, the FP2a-HA is harder to detect.

To assess parasite growth upon FP2a-HA knockdown, multi-cycle growth assays were conducted on both 3D7 WT and FP2a-HAglmS parasites. Trophozoite stage parasites were treated with increasing concentrations of GlcN over three consecutive cell cycles and harvested at each cycle to measure lactate dehydrogenase (LDH) activity as a proxy for parasite growth [52,53]. As expected, there was no substantial growth reduction observed in the FP2a-HAglmS knockdown parasites relative to untreated (0 mM GlcN) parasites or the 3D7 WT control (S3E Fig). This concurs with previous FP2a knockout studies, where FP3 was able to rescue FP2a knockout parasites later in the cell cycle [54]. We did however see a slight but significant growth reduction for 3D7 WT in the second cycle of treatment for 1 mM GlcN and for FP2a-HAglmS third cycle of treatment for 0.5 mM GlcN. Since our subsequent experiments were completed during one cell cycle, the parasites were not affected.

## Knocking down PTEX's core components, PTEX150 and HSP101, causes a build-up of full-length Hb inside the parasite

To determine if reduced Hb peptides upon PTEX150-HA knockdown was due to either reduced Hb uptake, or reduced Hb digestion, we used western blot technique on both the PTEX150-HA<sub>glmS</sub> line, and an additional line in which the core PTEX component HSP101 was similarly tagged (HSP101-HA<sub>glmS</sub>) [55]. As a control for Hb digestion we utilised the FP2a-HA<sub>glmS</sub> parasite line, as well as 3D7 WT parasites as a negative control.

To complete these assays, synchronised trophozoite stage parasites (~24-hpi) were treated with 0, 0.15, 1 or 2.5 mM GlcN for one cell cycle and tightly synchronised with a 4-h invasion window as described for metabolomics assays above. At 24-hpi in the next cell cycle, the RBCs were subsequently lysed in 0.09% saponin to remove RBC Hb. The parasite pellets were washed extensively in phosphate buffered saline (PBS) to remove Hb contamination prior to western blot (Fig 2A and 2B). As expected, the 3D7 WT control showed minimal changes in Hb levels, whereas following knockdown of PTEX150-HA, HSP101-HA or FP2a-HA, full-length Hb (monomer globin) was found to accumulate inside the parasite. This accumulation was found to be inversely proportional to the level of knockdown; a reduction in PTEX150-HA, HSP101-HA or FP2a-HA proteins was associated with an increase in undigested Hb inside the parasite (Fig 2A and 2B). This trend was more noticeable for the higher concentration of GlcN, likely due to the assay not being as sensitive to detect subtle changes in Hb levels compared to metabolomics assays. Although the Hb-build up was only found to be significant for the HSP101-HA<sub>glmS</sub> and FP2a-HA<sub>glmS</sub> parasites when comparing % Hb build-up compared to untreated at 1 mM GlcN, PTEX150-HA showed a strong trend for Hb-build up with increased protein knockdown (Fig 2A and 2B). We were not able to establish a strong knockdown for either PTEX150-HA (40–50%) or HSP101-HA (~50%), which might be why we did not observe stronger increase in full-length Hb inside the parasite using western blot as a readout. FP2a-HA was however almost completely knocked down. We also performed a simple linear regression analysis, where all three parasite lines (PTEX150-HA<sub>glmS</sub>, HSP101-HA<sub>glmS</sub> and FP2a-HA<sub>glmS</sub>) showed significant regression slope for Hb build-up when protein expression was reduced (S6A Fig).

To complement our results, we completed IFAs on saponin-lysed parasites probed with antibodies against full-length Hb (monomer globin) (Fig 2C, 2D and 2E). Tightly synchronised 3D7 WT, PTEX150-HA<sub>glmS</sub>, HSP101-HA<sub>glmS</sub> or FP2a-HA<sub>glmS</sub> parasites were treated  $\pm$  1 mM GlcN and harvested at 24-hpi for IFA and probed with mouse anti-EXP2 (parasite boundary) and rabbit anti-human Hb (full-length Hb). PTEX150-HA<sub>glmS</sub>, HSP101-HA<sub>glmS</sub> and FP2a-HA<sub>glmS</sub> parasites showed significantly higher mean fluorescence intensity for Hb signal when treated with GlcN whilst 3D7 WT parasites showed no difference between treatments (Fig 2C and 2D). No significant difference was observed for the cell size analysed except for HSP101-HA<sub>glmS</sub> parasites, which were significantly smaller when treated with GlcN (Fig 2E).

As Hb is digested by the parasite, toxic by-products from this process are sequestered as haemozoin crystals, which can be observed by light microscopy [56]. We next investigated the presence of haemozoin crystals during conditional knockdown of PTEX components to see if the parasites had reduced capability of forming the crystals, which could indicate that Hb digestion is reduced. Specifically, either PTEX150-HA<sub>glmS</sub> or HSP101-HA<sub>glmS</sub> parasites were treated for one cell cycle  $\pm$  2.5 mM GlcN to reduce respective protein expression (S6B, S6C and S6D Fig). 2.5 mM GlcN treatment was used because it produces the largest degree of knockdown for *glmS*-tagged protein mRNAs without noticeably reducing the growth of non-tagged parasites (S2 and S4 Figs) [6,55]. Knockdown of both PTEX150-HA<sub>glmS</sub> and

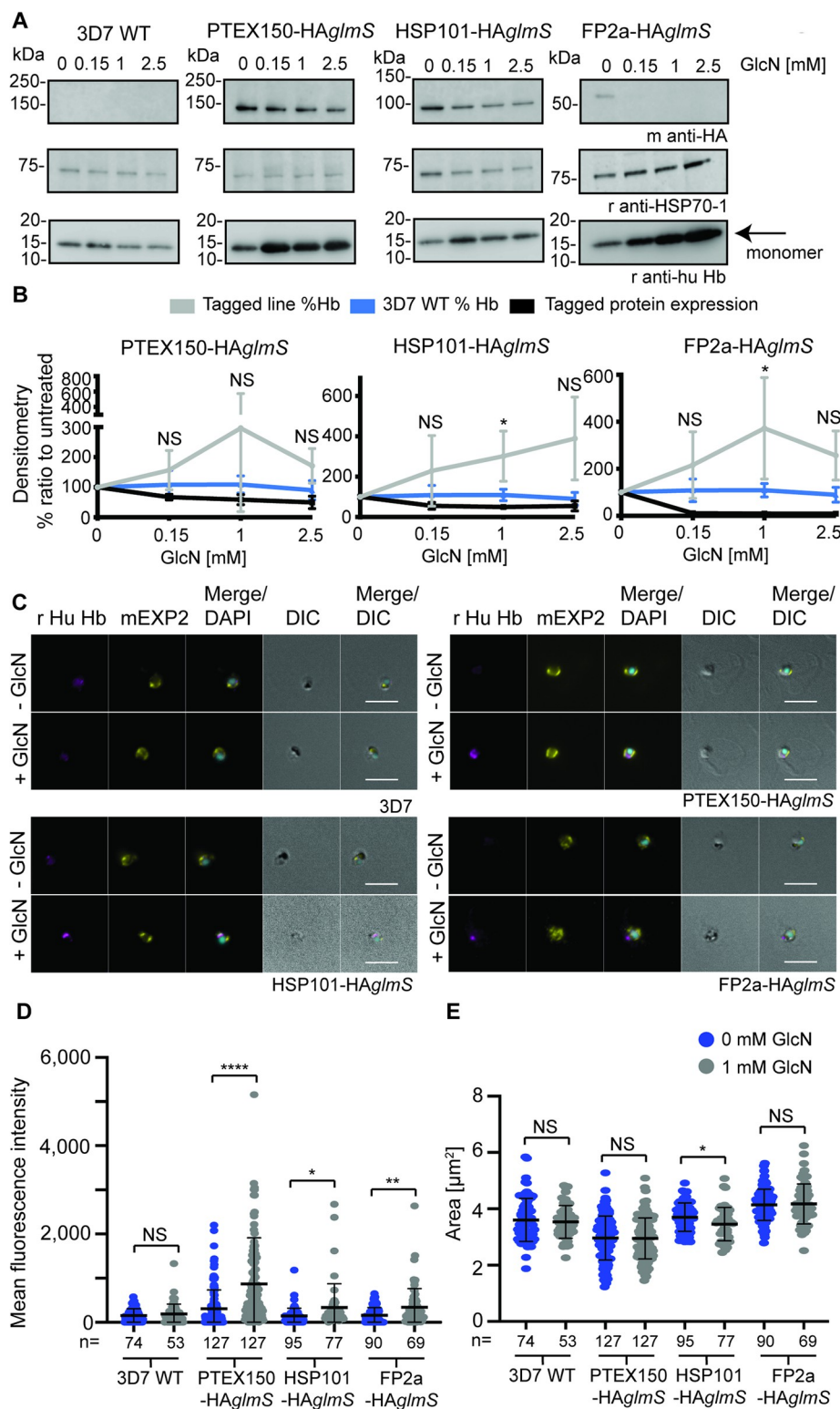


**Fig 2. Knockdown of PTEX150-HAglmS and HSP101-HAglmS results in build-up of full-length Hb inside the parasite.** (A) Trophozoite stage parasites were treated with 0, 0.15, 1 or 2.5 mM GlcN for one cell cycle, harvested via saponin lysis at ~24-hpi and prepared for western blot. Mouse anti-HA was used to probe for the target protein, rabbit anti-HSP70-1 was a loading control and rabbit anti-human Hb a marker for undigested Hb (monomer globin) inside the parasites. Blots are representative of 6 biological replicates for 0, 0.15 and 1 mM GlcN and 3 biological replicates for

2.5 mM GlcN condition. Full-length blots are shown in [S5 Fig](#). (B) Protein band densitometry of 6 (0, 0.15 and 1 mM GlcN) or 3 (2.5 mM GlcN) biological replicates was used to indicate the relative levels of Hb in the GlcN-induced knockdown parasites as a % ratio to untreated parasites. 3D7 WT was used as negative control and FP2a-HAglmS as a positive control for Hb build-up. The densitometry for Hb was done on the monomer (indicated with an arrow in panel A). The densitometry was taken as a ratio of the band of interest and the loading control. To measure the % of protein knockdown, the following formula was used: % knockdown = (GlcN treated / untreated) \* 100, where untreated was considered to have 100% expression. Error bars = SD. “%” refers to % build-up of Hb compared to untreated. Statistical analysis was completed for all GlcN conditions comparing 3D7 WT to PTEX150-HAglmS, HSP101-HAglmS and FP2a-HAglmS lines using Student’s t test with Welch correction. Only HSP101-HAglmS and FP2a showed significant increase in Hb levels compared to 3D7 WT, where (\*) indicates  $P = 0.0017$  (HSP101-HAglmS) and  $P = 0.0302$  (FP2a-HAglmS). However, PTEX150-HAglmS knockdown showed a trend towards Hb build-up inside the parasite when knocked down. (C) Highly synchronous 3D7 WT, PTEX150-HAglmS, HSP101-HAglmS and FP2a-HAglmS parasites were treated  $\pm$  1 mM GlcN for one cell cycle and 20 to 24-hpi trophozoites were lysed in saponin and prepared for IFA. Panels show representative figures from 2 (HSP101-HAglmS), 3 (3D7 WT and FP2a-HAglmS) or 4 (PTEX150-HAglmS) biological replicates. DAPI (4',6-diamidino-2-phenylindole) was used to stain the nucleus. DIC = differential interference contrast. Scale bars = 5  $\mu$ m. (D) The mean fluorescence of the parasite cells in panel C was measured in the Hb channel, where the area measured was denoted by the boundary of the EXP2 channel. The mean fluorescent intensity was then calculated and statistical analyses were completed using Student’s t test with Welch correction, where the number of cells analysed is indicated below the graph. A significant increase in Hb mean fluorescent intensity was observed when PTEX150-HAglmS, HSP101-HAglmS and FP2a-HAglmS parasites were treated with 1 mM GlcN compared to 0 mM GlcN, where NS indicates  $P = 0.3740$ , (\*\*\*\*) indicates  $P < 0.0001$ , (\*) indicates  $P = 0.0231$  and (\*\*) indicates  $P = 0.0013$ , and error bars = SD. 3D7 WT ( $P = 0.3740$ ) did not show significant difference between treatment conditions. (E) Cells analysed in panel D were of similar size where Student’s t test with Welch correction showed that there was no significant difference between treatments, except for HSP101-HAglmS parasites, where (\*) indicates  $P = 0.0192$ . Middle line represents mean and error bars = SD.

<https://doi.org/10.1371/journal.ppat.1011006.g002>

HSP101-HAglmS parasites resulted in significantly less haemozoin crystal formation ([S6B](#) and [S6C Fig](#)) indicating less Hb was being digested which concurs with western blot results and IFA data above ([Fig 2](#)). There was a significant reduction in cell size for the PTEX150-HAglmS parasites used for the analysis but not for HSP101-HAglmS ([S6D Fig](#)). Both parasite lines showed a growth delay during 2.5 mM GlcN treatment as evident by Giemsa-stained smears ([S2](#) and [S4](#) Figs). No significant difference was observed for 3D7 WT or FP2a-HAglmS parasites when treated with 2.5 mM GlcN ([S6B](#), [S6C](#) and [S6D](#) Figs). FP2a knockdown parasites sometimes appeared to have smaller crystals ([S6B Fig](#)) and expansion of the food vacuole ([S2](#) and [S6E](#) Figs, arrows) like that observed in previous FP2a knockout studies [[47,54](#)]. This expansion of the food vacuole was sometimes observed in PTEX150-HAglmS and HSP101-HAglmS knockdown lines but was less prominent compared to the FP2a-HAglmS knockdown ([S2](#) and [S4](#) Figs, arrows). Collectively these data demonstrate that upon knockdown of the PTEX components PTEX150-HA and HSP101-HA, parasites still take up Hb. However, the parasites are unable to properly digest Hb and we therefore hypothesised that PTEX may be involved in the trafficking of proteases involved in the degradation of Hb, and likely not the process by which the Hb is taken into the parasite.

### Generation of FP2a trappable reporter cargoes to investigate FP2a relationship with PTEX

Next, we sought to better understand the relationship between PTEX and Hb digestion. To this end, we generated a series of FP2a reporter constructs to investigate the reporters’ trafficking and interaction with PTEX *en route* to the food vacuole as the protease is thought to traffic to the food vacuole via the cytostome at the PPM/PVM interface [[34,35,45](#)]. It should be noted that both FP2a and plasmepsin II (discussed later) are synthesised as an integral type II membrane pro-enzymes that are later cleaved into the mature protease (active form) by removal of the N-terminus pro-segment in the acidic environment of the food vacuole, or by protease cleavage [[45,57,58](#)]. The N-terminus helps direct the pro-enzyme from the ER to the food vacuole [[34,35](#)]. Here, three FP2a reporters of differing lengths were generated, all appended to a

nanoluciferase (Nluc) ultra-bright bioluminescence reporter [59], murine dihydrofolate reductase domain (DH) [60] and a triple FLAG (FL) epitope tag. The initial two constructs included the first 120 or 190 aa of FP2a, here referred to as “120 aa” and “190 aa”, respectively (Fig 3A). Previous truncation studies demonstrated that the first 105 aa of FP2a are sufficient for its trafficking to the food vacuole [35], however a construct containing the first 120 aa was more efficiently trafficked to the food vacuole which is why this length was chosen here [34,35]. The longer 190 aa version was made to investigate if an N-terminus longer than 120 aa would provide more efficient trafficking to the food vacuole. A third reporter was generated as a negative control and contained the N-terminal trafficking region of FP2a but lacked the N-terminal TM domain (Fig 3A) required for entry into the secretory pathway [34,35] and subsequent trafficking to the food vacuole. This reporter is referred to as “NT” throughout the text (Fig 3A).

By adding an antifolate ligand such as WR99210 we can stabilise the globular domain of DH and thereby inhibit the reporter proteins from unfolding. The DH domain has been previously utilised to study both mitochondrial protein import [60] and protein export in malaria parasites [61–63]. PTEX requires cargo to be unfolded prior to export [61] and therefore if FP2a is trafficked via PTEX, the 120 and 190 aa reporters should become trapped at the PTEX when inhibited from being unfolded via addition of WR99210 as previously observed for exported protein reporters [62,63].

All reporters were episomally expressed in the HSP101-HAglmS parasite background, under the *ef1a* promoter (Fig 3A). They were successfully detected by western blot, where they migrated at the expected sizes (Fig 3B). Additionally, IFA analysis confirmed that the 120 and 190 aa reporters were trafficked to the food vacuole where they co-localised with the haemozoin crystals whilst the NT reporter displayed a diffuse signal within the parasite cytoplasm, as expected (Figs 3C and S8, left panels). Both the 120 and 190 aa reporters showed localisation to the ER, which is expected as they are under the *EF1a* promoter and continuously being trafficked from the ER (Figs 3C and S8). The 190 aa reporter however appeared to be more concentrated at the food vacuole than the 120 aa reporter indicating that the longer N-terminus could enable more efficient trafficking to the food vacuole (Figs 3C and S8). Brefeldin A (BFA), which blocks protein secretion from the ER to the Golgi [64,65], was also used to confirm that the reporters were secreted from the ER as happens for the native protease [34,35]. In the presence of BFA the 120 and 190 aa reporters were retained within the ER whilst no changes were observed for the distribution of the NT reporter as expected (Fig 3D). Both the 120 and 190 aa reporters localised to the parasite periphery and cytoplasm rather than being concentrated in the food vacuole which is due to the use of younger parasites for this experiment. Overall, these data confirm that the reporters are expressed and appropriate for use in subsequent experiments.

### The FP2a 120 aa reporter displays increased co-localisation with EXP2 when inhibited from unfolding

To determine if FP2a associates with PTEX, the 120 aa, 190 aa and NT reporters were trapped using WR99210 and IFAs were performed to detect co-localisation with PTEX components at the PVM. Tightly synchronised (4-h window) ring stage parasite cultures (~12-hpi) were treated  $\pm$  10 nM WR99210 and harvested at trophozoite stage (24 to 28-hpi) for IFA. Rabbit anti-Nluc was used to visualise the FP2a reporters and mouse anti-EXP2 served as both a PTEX and PVM marker (Figs 4A and S8). The 120 and 190 aa reporters displayed some labelling around the parasite surface/PVM, which was expected as early acting Hb proteases are known to traffic there for loading into the cytostome prior to delivery to the food vacuole [34–

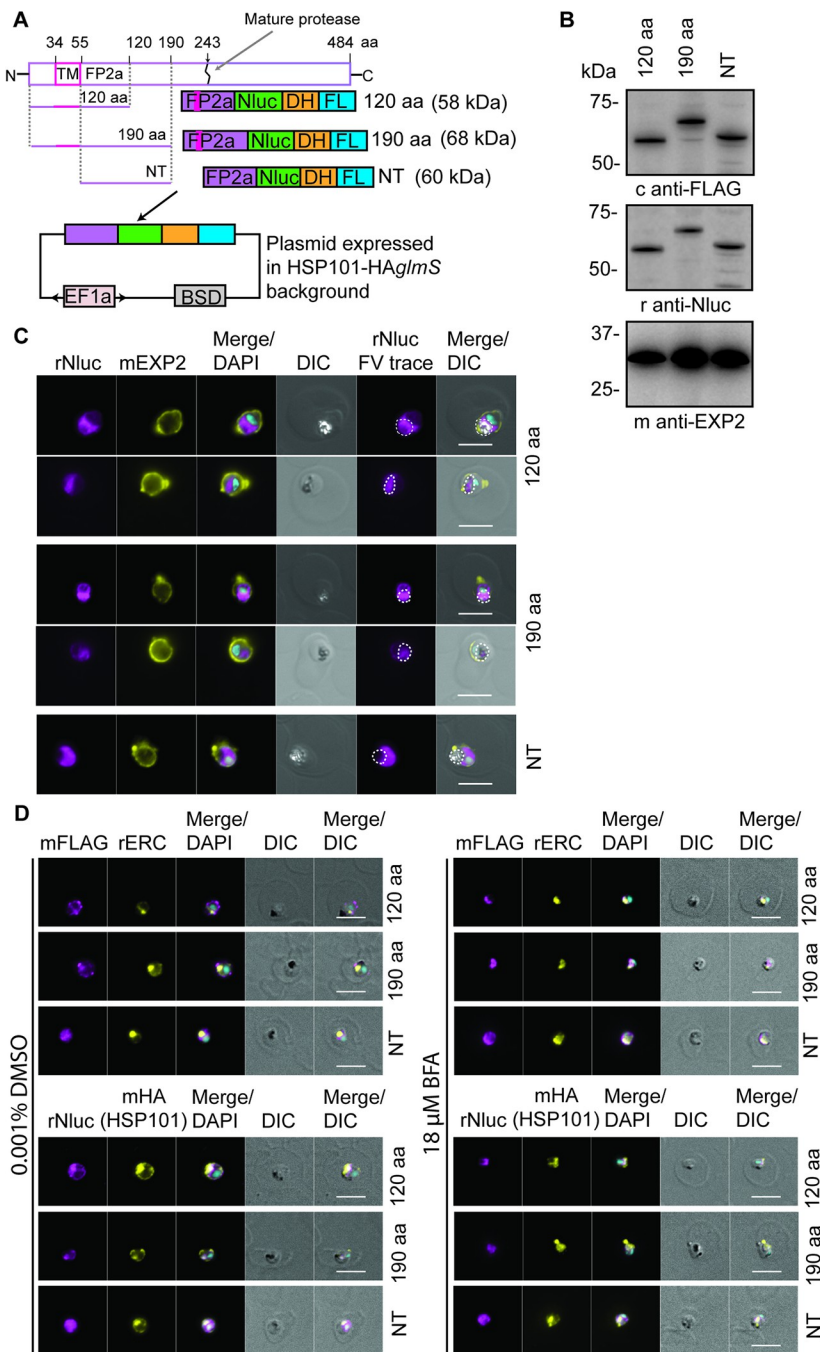


**Fig 3. FP2a trappable reporters were generated to study the relationship of FP2a with PTEX.** (A) Three FP2a reporters were generated. 120 aa and 190 aa containing the first 120 aa and 190 aa of FP2a respectively. The NT reporter refers to the 190 aa reporter without the N-terminal TM domain and served as a negative control. All FP2a sequences were appended with nanoluciferase (Nluc), murine dihydrofolate reductase (DH) and a 3x FLAG (FL) epitope tag. The complete protein map for FP2a is indicated above for reference, where the reporter only contains the N-terminus sufficient for food vacuole delivery and not the C-terminus necessary for protease activity. The reporters were episomally expressed from a plasmid under the bidirectional EF1a promoter in the HSP101-HAglmS parental line and maintained under Blasticidin-S selection via the Blasticidin-S Deaminase (BSD) cassette. (B) Western blot analysis demonstrated that the 120 aa, 190 aa and NT FP2a reporters are expressed and migrate at the correct size indicated in panel A. Rabbit anti-Nluc was used to detect the Nluc tag and chicken anti-FLAG to detect the FL tag. Mouse anti-EXP2 was used as a loading control. Full-length blots are shown in S7 Fig. (C) Immunofluorescence assays show that the 120 aa and 190 aa FP2a reporters are trafficked to the food vacuole. The NT FP2a reporter displayed diffuse labelling within the parasite as expected. Rabbit anti-Nluc was used to detect the reporter, mouse anti-EXP2

was used as a PVM marker and haemozoin crystals in the DIC show food vacuole (FV) localisation (indicated with a white dotted line). (D) Late ring/early trophozoites were treated  $\pm$  18  $\mu$ M BFA to inhibit ER to Golgi protein secretion. The 120 and 190 aa FP2a reporters were both trapped in the ER upon BFA treatment as expected and no changes were observed for the NT reporter. Rabbit anti-ERC was used as an ER marker and mouse anti-HA to label for HSP101-HA<sub>glmS</sub>, which also traps in the ER upon BFA treatment [55]. DAPI was used to stain the nucleus. Scale bars = 5  $\mu$ m.

<https://doi.org/10.1371/journal.ppat.1011006.g003>

36]. To quantify the co-localisation of reporters with EXP2  $\pm$  WR99210, Pearson's coefficients of the proteins were measured (Fig 4B). The 120 aa co-localised significantly more with EXP2 when treated with WR99210 indicating that more cargo was trapped at the parasite periphery when rendered unfoldable and therefore potentially trapped at the PTEX (Fig 4A and 4B). However, the 190 aa and NT reporters did not show a significant difference in co-localisation with EXP2  $\pm$  WR99210 treatment (Fig 4A and 4B). Since the 120 and 190 aa reporters are identical except for their length, it is likely that length is influencing trapping efficiency and that shorter cargo is more easily trapped (discussed in later sections).

Interestingly, even though the 120 aa cargo co-localised with EXP2, it was never observed inside so-called “EXP2 loops” (Fig 4A, white arrows) which we commonly observe for the exported reporter Hyp1-Nluc-DH upon WR99210 trapping [63,66]. These loops are extensions of the PVM, likely representing the tubulo-vesicular network, and are thought to contain accumulated trapped cargo unable to be transported by the PTEX complex at the PVM [63]. The absence of the FP2a reporter cargo from these loops could indicate that it might not be trapped at the PVM, but instead at the PPM. We sought to further investigate the putative interaction between PTEX and FP2a using co-immunoprecipitation assays (Co-IPs).

### Both the 120 aa and the 190 aa reporters associate with PTEX core components, but this association is diminished when reporters are inhibited from unfolding

To investigate the interaction between HSP101-HA and FP2a, Co-IPs were performed with the three FP2a reporters (NT, 120 aa, 190 aa). We also employed an exported protein reporter, Hyp1-Nluc-DH-FL or “Hyp1”, as a positive control for PTEX interaction [55]. Synchronised ring stage parasites (~12-hpi) were treated  $\pm$  10 nM WR99210 and trophozoite stage iRBCs (28–32-hpi) were isolated from uninfected RBCs (uRBCs) by magnet purification. This time point was chosen because it was when the FP2a and Hyp1 reporter proteins were optimally expressed (S9 Fig) [55]. Parasite lysates were incubated with anti-HA agarose beads to immunoprecipitate (IP) HSP101-HA and its interacting proteins for visualisation by western blot (Fig 5A).

As expected, the Hyp1 reporter showed an increased association with HSP101-HA when treated with WR99210 reflective of the folded cargo becoming trapped at the PTEX under these conditions [55,63] (Fig 5A, lanes 9 and 10, 5B and 5C). The NT reporter showed a minimal level of association with HSP101-HA (Fig 5A, lanes 11 and 12, 5B and 5C) as expected. Importantly, both the 120 and 190 aa reporters showed an enhanced association with HSP101-HA in the absence of WR99210, demonstrating that FP2a does indeed interact with HSP101-HA (Fig 5A, lanes 13–16, 5B and 5C). It should be noted that a marked difference was observed between the retention of the 120 and 190 aa reporters (Fig 5A lanes 13 and 14 vs. lanes 15 and 16) with HSP101-HA, whereby substantially more of the 120 aa reporter is bound by HSP101. This concurs with the greater trapping efficiency of the 120 aa reporter at the parasite periphery with EXP2 as visualised by IFA (Figs 4 and S8).

It was anticipated that in the presence of WR99210, the reporters would be more strongly associated with HSP101-HA if they were trapped at the PVM-resident PTEX, but instead the

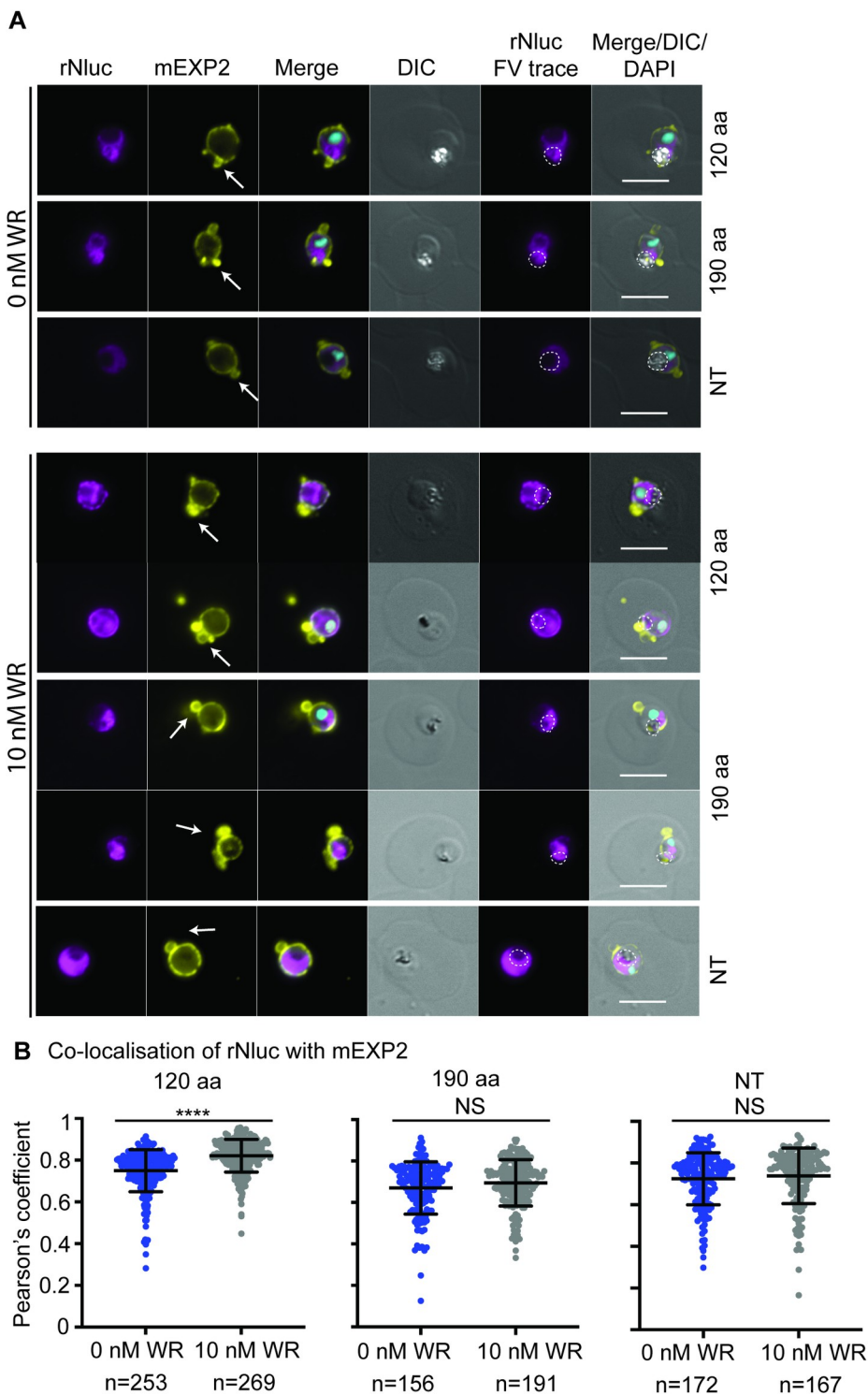


**Fig 4. The FP2a 120 aa reporter shows significantly more association with EXP2 upon WR99210 trapping.** (A) Highly synchronous parasites expressing the 120 aa, 190 aa and NT FP2a reporters were sorbitol synchronised at ring stage and treated  $\pm$  10 nM WR99210 to prevent unfolding of the reporters to see if they would become trapped at the parasite periphery with PTEX. When treated with WR99210, more 120 aa reporter was observed at the PPM/PVM indicating its trafficking was affected. No substantial difference was observed for 190 aa or NT reporters. Shown are representative images for 3 (120 aa) and 2 (190 aa and NT) biological replicates. Rabbit anti-EXP2 was used as a PVM marker, rabbit anti-Nluc to detect the reporters and DAPI to stain the nucleus. FV = food vacuole. Scale bars = 5  $\mu$ m.

Arrows point to PVM loops. (B) Pearson's coefficient was used to measure the co-localisation of the FP2a reporters (Nluc) and EXP2. There was significantly more co-localisation of 120 aa with EXP2 when treated with WR99210 as determined by student's t test with Welch correction but no significant difference was observed for the 190 aa or NT reporters. (\*\*\*\*) Indicates  $P < 0.0001$ ,  $n =$  cells analysed (pooled from 3 (120 aa) or 2 (190 aa and NT) biological replicates), middle line on the graph represents mean and error bars = SD. Each dot on the graph represents a cell analysed.

<https://doi.org/10.1371/journal.ppat.1011006.g004>

association of the reporters with HSP101-HA was reduced (Fig 5A, lanes 13–16, 5B and 5C). These data therefore imply that when 120 and 190 aa reporter proteins are inhibited from unfolding they might in fact be trapped in the PPM prior to PTEX association in the PV as has

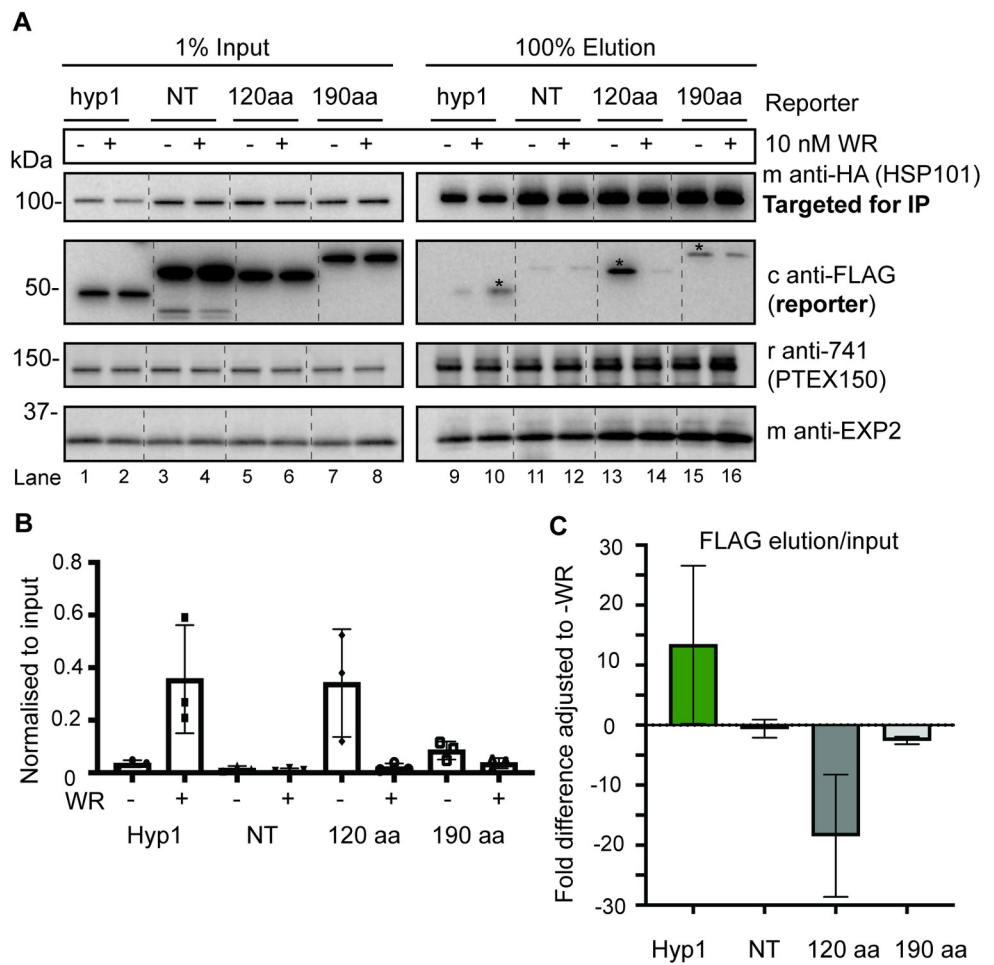


**Fig 5. Both the 120 aa and the 190 aa FP2a reporters interact with HSP101-HA and this interaction is weaker when reporters are inhibited from unfolding via addition of WR99210.** (A) Ring stage HSP101-HA<sub>AgmS</sub> parasites episomally expressing Hyp1, NT, 120 aa, or 190 aa reporters were treated  $\pm$  10 nM WR99210 and harvested at trophozoite stage (~28 to 32-hpi). Anti-HA IgG beads were used to IP HSP101-HA and its interacting proteins. Input shows 1% protein lysate used for the assay, and elution refers to protein bound to the HA beads/HSP101-HA indicating their interaction with HSP101-HA. Hyp1 was used as positive control and NT as a negative control. Mouse anti-HA was used to probe for HSP101-HA, chicken anti-FLAG for the reporter, rabbit anti-741 for PTEX150 and mouse anti-EXP2 for EXP2. Blot is representative of 3 biological replicates. The asterisks indicate stronger signal when comparing the  $\pm$  WR99210 treatment for respective reporter as determined by densitometry of all biological replicates. Full-length blots are shown in S10 Fig. (B) The interaction of reporters with HSP101-HA was graphed, where FLAG elution was adjusted to input. Each dot represents 1 biological replicate. (C) The interaction of reporters with HSP101-HA, where the fold difference of the FLAG elution/input was adjusted to untreated (-WR99210). Error bars = SD from 3 biological replicates.

<https://doi.org/10.1371/journal.ppat.1011006.g005>

been observed for PNEPs [62]. This explains why we did not observe the FP2a reporters in PVM loop extensions by IFA (Fig 4A) as mentioned above, which have previously been shown to contain PTEX-trapped exported reporter protein [63].

Association of the FP2a reporters was also confirmed for PTEX150 and EXP2 by Co-IPs using either rabbit anti-PTEX150 (r942) (S11A Fig) or rabbit anti-EXP2 (r1167) (S11B Fig) antibodies. PTEX150 showed stronger association with the 120 and 190 aa FP2a reporters compared to HSP101-HA, this was particularly the case for the 190 aa reporter (S11A Fig, lanes 13–16 and S12A Fig) and a weak association was observed for the cargoes with EXP2 (S11B Fig, lanes 13–16 and S12B Fig). Densitometry measurements showed a similar trend for the association of Hyp1 and FP2a reporters with both PTEX150 and EXP2 when compared with HSP101-HA IPs (S12 Fig). Overall, these assays helped to confirm that FP2a interacts with PTEX, as was suggested by our metabolomics and Hb digestion/build-up assays.

### The FP2a 120 aa reporter becomes trapped at the PPM with the N-terminus facing into the PV compartment when inhibited from unfolding

Given that the 120 aa reporter cargo displayed an increased co-localisation with EXP2 by IFA when inhibited from unfolding (Figs 4B and S8) but showed reduced association with PTEX components when trapped with WR99210 (Figs 5 and S11), we used proteinase K protection assays to determine which iRBC compartment the reporter was being trapped in. For the assay, synchronised ring stage parasites (~12-hpi) were treated  $\pm$  10 nM WR99210, prior to harvesting at the trophozoite stage (~24 to 28-hpi) via magnet purification. Isolated trophozoite-containing RBCs were treated with equinatoxin-II (EQT) to form pores in the iRBC membrane [67] and release soluble exported proteins (Fig 6A, lanes 1 and 6). The subsequent iRBC pellet was then divided into four fractions that were untreated, treated with proteinase K, or subjected to differential lysis conditions and proteinase K treatment. Saponin was used to lyse the parasite's PVM, releasing the PV contents (Fig 6A, lanes 4 and 9) and Triton X-100 (TX-100) was used to lyse all membranes (Fig 6A, lanes 5 and 10). Specific antibodies were then used as markers for each lysed compartment, where GBP130 was used as a soluble exported protein marker [63,68], SERA5 as a soluble PV marker [69] and GAPDH as a marker of the parasite cytoplasm.

By analysing the distribution of FP2a bands across all treatments, it was possible to infer the orientation and localisation of the 120 aa reporter protein. Firstly, the reporter protein was minimally degraded in the PBS and proteinase K condition, but we often observed weaker signal for the SERA5 control when comparing PBS pellet with PBS + proteinase K and conclude that this is likely due to a breakage of the PVM in minority of parasites. This indicates that the reporter does not reside within the iRBC cytoplasm, which concurs with our IFA data (Figs 6A, lanes 3 and 8 and 4A). FP2a is a type II integral membrane protein transiently present at the PPM and is not inserted into the PVM extending into the RBC compartment [70]. Concordantly, when the parasites were treated with saponin and proteinase K, the FP2a reporter was estimated to migrate 3.8 kDa smaller than the full-length reporter, as measured by the Odyssey LI-COR Image Studio software using the molecular marker for reference (Fig 6A, lanes 4 and 9). This 3.8 kDa fragment is proportional to the segment of the reporter protein that precedes the N-terminal TM domain (4 kDa) suggesting that FP2a is oriented with its N-terminus facing into the PV lumen, and the C-terminus is in the parasite cytoplasm (Fig 6C). The FP2a reporter was completely degraded in the presence of TX-100 indicating that the parasite membranes were completely permeabilised (Fig 6A, lanes 5 and 10), however, GAPDH was not degraded. This is likely because GAPDH is highly abundant and proteolytically resistant.

Following WR99210 treatment, the FP2a reporter parasites that were lysed with saponin and treated with proteinase K revealed that the reporter was more resistant to degradation

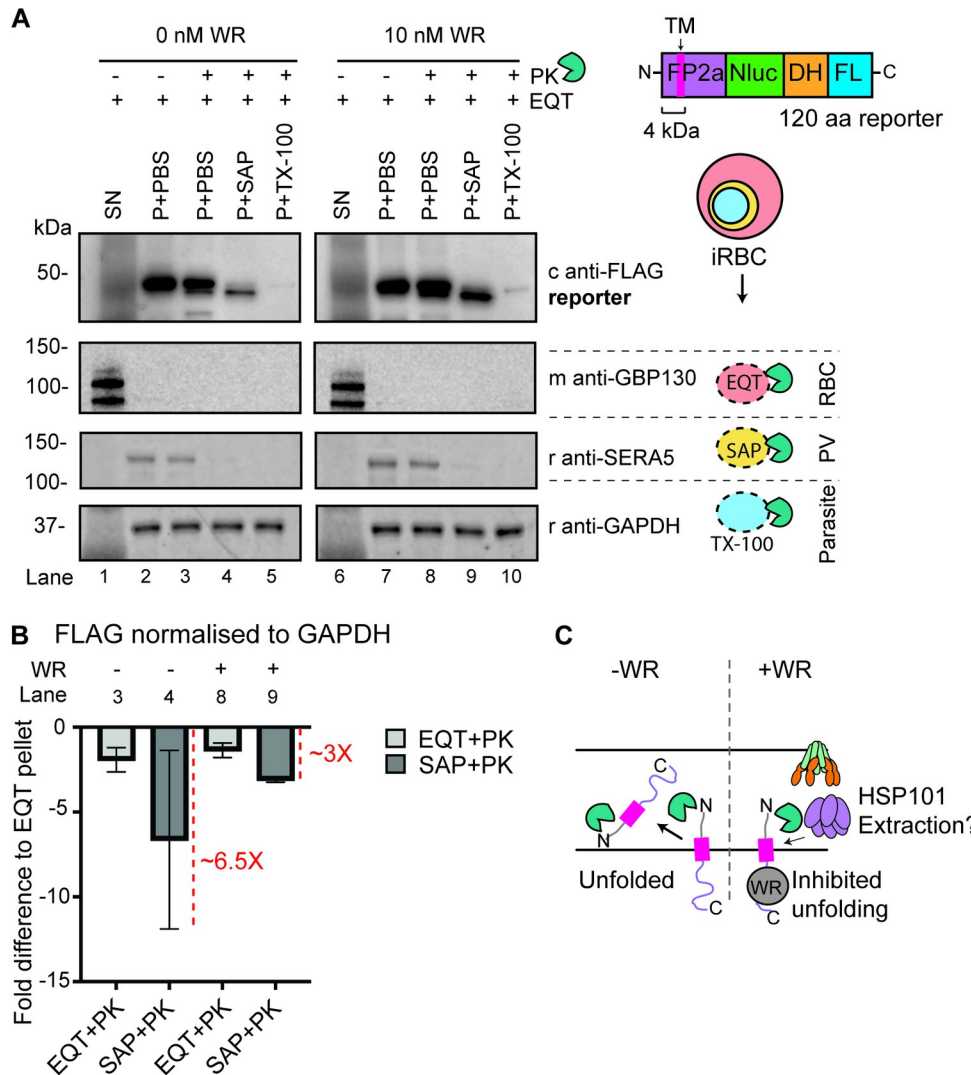


**Fig 6. Proteinase K protection assay shows that FP2a needs to be unfolded before crossing the PPM with its N-terminus first.** (A) Ring stage parasites were treated  $\pm$  10 nM WR99210 to inhibit the 120 aa FP2a reporter from unfolding. Trophozoite stage parasites were magnet purified and used for proteinase K (PK) protection assays. EQT was used to permeabilise the iRBC membrane, saponin (SAP) to lyse the PVM, and TX-100 to lyse all membranes. A 3.8 kDa shift was observed in the reporter size when the PV was lysed and treated with PK (lanes 4 and 9), which matches the predicted size of the 34 aa (4 kDa) N-terminus preceding TM domain (measured in Odyssey LI-COR). FP2a reporter appears to be more protected against PK degradation when treated with WR99210 vs non-treated, indicating trapping at the PPM not PVM. Chicken anti-FLAG was used to probe for the FP2a reporter, GBP130 is a soluble exported protein marker, SERA5 is a PV marker and GAPDH is a parasite cytoplasm marker. Blot is representative of 3 biological replicates, which showed a similar trend, SN = supernatant, P = pellet. Full-length blots are shown in S13 Fig. (B) The fold difference for protection of the FP2a reporter (FLAG) was measured by densitometry, where the FLAG signal was adjusted to GAPDH and the fold difference measured by adjusting the EQT + PK and SAP + PK signal to EQT + PBS. The fold difference (X) compared with untreated is indicated with a red dotted line on the graph. Error bars = SD from 3 biological replicates. (C) A suggested model derived from the PK assay results. When parasites were not treated with WR99210 more reporter cargo was degraded indicating that when inhibited from unfolding the reporter was trapped at the PPM, likely inhibiting extraction into the PV potentially facilitated by HSP101 as suggested for exported proteins with a transmembrane domain.

<https://doi.org/10.1371/journal.ppat.1011006.g006>

than it was in the absence of WR99210 (Fig 6A and 6B, lanes 3 and 4 vs. lanes 8 and 9) suggesting that FP2a needs to be unfolded before crossing the PPM and entering the PV compartment. This demonstrates that the WR99210 trapping occurs at the PPM interface prior to

PTEX association within the PV, which agrees with our IP data where FP2a shows less interaction with PTEX components when treated with WR99210 (Figs 5 and S11). This could also explain why the 190 aa reporter is more efficiently trafficked to the food vacuole, since the length of the N-terminus has been shown to be important for PPM extraction of exported TM domain containing proteins into the PV [62].

### PTEX150 co-precipitates native plasmeprin II Hb protease and PTEX150-HAglmS knockdown affects protease trafficking

To study the relationship between PTEX and a native Hb protease, we tagged the early acting Hb protease plasmeprin II (PM II, PF3D7\_1408000) with mScarlet as described for FP2a-HAglmS above (S15A Fig), however, the background line used for transfection of this line was PTEX150-HAglmS. Integration was confirmed by PCR (S15B Fig). A single band of 75 kDa was detected for PM II-mScarlet by western blot, where the tag accounted for approximately 27 kDa (Fig 7A). This agrees with previously published results using a PM II-GFP reporter, where only the pro-form of the protease was detected by an anti-GFP antibody and not the mature cleaved protease [36]. Live cell microscopy confirmed the localisation of PM II-mScarlet during ring and trophozoite stage, where the protease co-localised with the haemozoin crystals (Fig 7B, white dotted line) as expected. To determine if PTEX is involved in PM II trafficking, we knocked down PTEX150-HAglmS mRNA expression at the trophozoite stage and harvested cells for microscopy at the following late ring stage (~20-hpi). We observed a significant accumulation of PM II-mScarlet at the parasite periphery when PTEX150-HA was knocked down (crescent/circle) compared to a peripheral ‘dot’ when PTEX150-HA was normally expressed (Fig 7C and 7D). While this is qualitative evidence for a role for PTEX150 in PM II-mScarlet trafficking to the food vacuole, some observations could merely represent PM II-mScarlet during its normal trafficking to the cytostome via the parasite periphery. To support that our observations are indeed due to an interaction with PTEX150, we targeted PTEX150-HA for IP using anti-HA agarose beads as previously described. A strong association was seen between PTEX150-HA and PM II-mScarlet (Fig 7E). Positive control antibodies against HSP101 and EXP2 also revealed that they too associated with PTEX150 as expected, while rabbit anti-GAPDH was used as a negative control and showed no association (Fig 7E). 3D7 WT parasites were used to detect any non-specific antibody binding in the assay and showed no interaction with PTEX150 or other PTEX components. Overall, this assay confirmed a specific association between PTEX and a native Hb protease (PM II-mScarlet) and complements our FP2a reporter data.

## Discussion

This study sought to elucidate why PTEX is essential by determining which metabolic pathways were perturbed due to the failure to export proteins into the iRBC compartment when the protein components of PTEX were knocked down. Hundreds of parasite proteins are exported into the iRBC, but we do not know what most of these proteins do and why some of them are essential. Metabolomic analyses revealed that knockdown of PTEX150-HA caused a slight dysregulation of some metabolite levels, for example those involved in glycolysis and nucleotide metabolism, however this was also observed in the 3D7 WT control indicating a non-specific effect from the GlcN treatment. The only clearly defined effect of PTEX150-HAglmS knockdown was upon Hb digestion, possibly linking the PTEX machinery to this essential catabolic process that provides the parasite with amino acids and helps maintain osmotic stability of the iRBC [33,40–42]. Using several approaches, we were able to determine a physical connection between PTEX and two major early acting Hb proteases, FP2a and PM

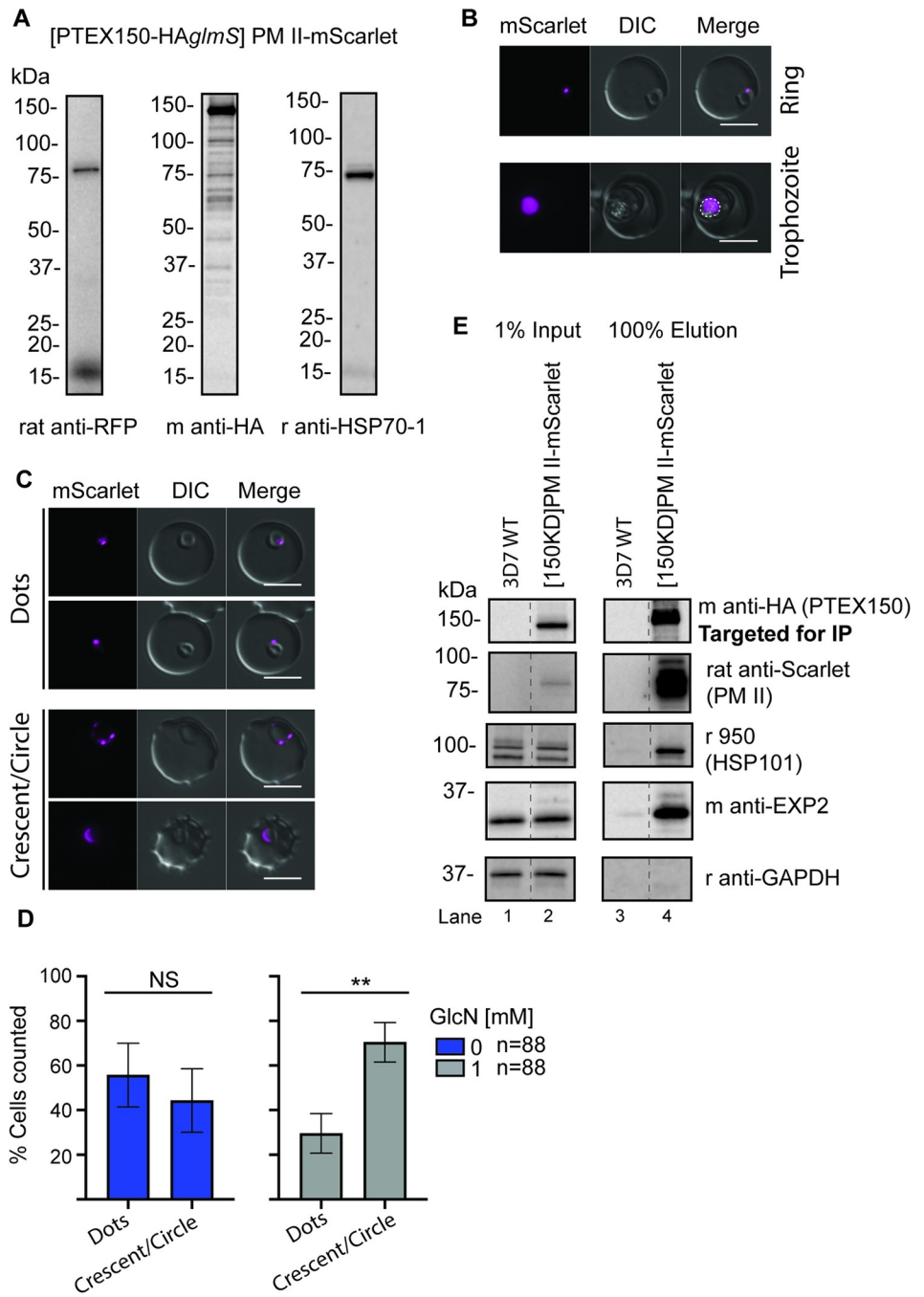


**Fig 7. The PM II-mScarlet fusion protein in the PTEX150-HAglmS parental line accumulates at the parasite periphery when PTEX150-HA is knocked down and co-precipitates with PTEX150-HA.** (A) Western blot was used to confirm the correct size of PM II-mScarlet, detected by rat anti-RFP (red fluorescent protein), which detects the mScarlet tag. Mouse anti-HA was used to detect the PTEX150-HA of the parental line and rabbit anti-HSP70-1 was used as a loading control. Only the pro-form of the protease was detected. (B) Live cell microscopy was used to visualise the localisation of the mScarlet (PM II) in both ring and trophozoite stage parasites, where the tag was observed inside the parasite and overlapping with the food vacuole (haemoglozin crystals), which are indicated with a dotted white line. Scale bars = 5 μm. (C) PM II-mScarlet parasites were treated ± 1 mM GlcN at trophozoite stage and harvested at late ring/early trophozoite stage (~20-hpi) for live cell microscopy. The mScarlet signal was subsequently categorised as either 'dot' or 'crescent/circle' around the parasite periphery. Panel shows representative images for each category, the experiment was completed in 3 biological replicates. Scale bars = 5 μm. (D) Graphs show the percentage of parasites with dots vs. crescent/circular labelling from the experiment in panel C. Statistical analysis was completed using Student's t test with Welch correction. n = total number of cells counted per condition with 3 biological

replicates combined. Error bars = SD for 3 individuals counting. (\*\*) Indicates  $P = 0.0048$ . (E) Anti-HA IgG beads were used to IP PTEX150-HA and its interacting proteins. EXP2 and HSP101 were used as positive control for interaction, GAPDH as a negative control and 3D7 WT as a negative control for non-specific interaction with beads. Blot is representative of 2 biological replicates. Full-length blots are shown in [S14 Fig](#).

<https://doi.org/10.1371/journal.ppat.1011006.g007>

II. It is possible that these Hb proteases might rely on PTEX components as they transit via the PPM *en route* to the cytostome [34–36].

Modest knockdown of PTEX150-HA<sup>gms</sup> with 1 or 2.5 mM GlcN reduces PTEX150-HA expression to ~40–50% of normal levels (in our study) and arrests growth at the late ring / early trophozoite stage in the cycle following addition of GlcN ([S2 Fig](#)) [6]. As the degree of growth inhibition would also likely produce many metabolic defects, we also used 0.15 mM GlcN, which does not arrest parasite growth ([S2](#) and [S4](#) Figs) [6]. This treatment also resulted in a reduction in Hb digestive peptides detected by metabolomics and western blot, and microscopy analysis demonstrated the reduction was likely due to diminished capacity to digest Hb rather than a defect in total Hb uptake. This contradicts results presented in a recent study by Gupta *et al.*, where they observed less Hb uptake in HSP101 knockdown parasites [71]. Their study was however performed differently to ours whereby HSP101 expression was knocked down from late trophozoite stage of the first cycle to the early schizont stage of the next cycle (42 to 44-hpi). This could result in the HSP101 knockdown parasites stalling at the early trophozoite stage of the second cycle and therefore not being able to take up as much Hb as the untreated control parasites which had continued growing and transitioned into the schizont stage. This trophozoite stalling effect due to functional inactivation of HSP101 has been previously noted using the same HSP101 knockdown line [5]. Interestingly we did observe that Hb build-up inside the parasite did not always correlate directly with the localisation of the haemozoin crystals by microscopy. This could suggest that there is some trafficking defect of Hb within the parasite cytoplasm to the food vacuole, potentially due to proteins trafficked by PTEX that have a role in its delivery. This however needs to be explored further in more detail.

To determine if PTEX knockdown was inhibiting the delivery of Hb proteases to cytostomal vesicles we used FP2a reporter cargo constructs, which allowed us to study the interactions between PTEX and this early acting Hb protease. The FP2a 120 aa and 190 aa reporters were directly co-precipitated with PTEX core components, although much stronger with HSP101 and PTEX150 than EXP2. If the N-terminus of the FP2a reporter that is projecting into the PV (34 aa) is interacting with the PTEX complex, it likely associates more with HSP101 and PTEX150 than EXP2, which is further away ([Fig 8](#)). The slightly weaker association with EXP2, that was also observed for the positive control Hyp1, could be due to IP efficiency. EXP2 has a dual function; as a channel in the PTEX complex and as a nutrient channel on the PVM [11,72]. This dual function could therefore influence the co-IP of EXP2 with FP2a and Hyp1, as the pool of nutrient channel related EXP2 is not associated with PTEX functioning. Importantly, each assay co-precipitated the other members of the PTEX suggesting involvement of the full PTEX complex in protease binding ([Figs 5](#) and [S11](#)) and a similar trend was observed for HSP101, PTEX150 and EXP2 IPs with reporter cargoes ([Figs 5B, 5C](#) and [S12A and S12B](#)). Importantly, this association was also observed for a native early acting Hb protease, PM II, suggesting PTEX's interaction with FP2a reporters reflected genuine trafficking interactions ([Fig 7E](#)). It is plausible that the FP2a reporters are interacting directly with one or two PTEX component and indirectly co-precipitating other core component/s. It should be noted that conditionally inhibiting the function of HSP101 did not reduce the proteolytic processing of native PM II [5] that normally occurs in the food vacuole facilitated via FP2 and FP3

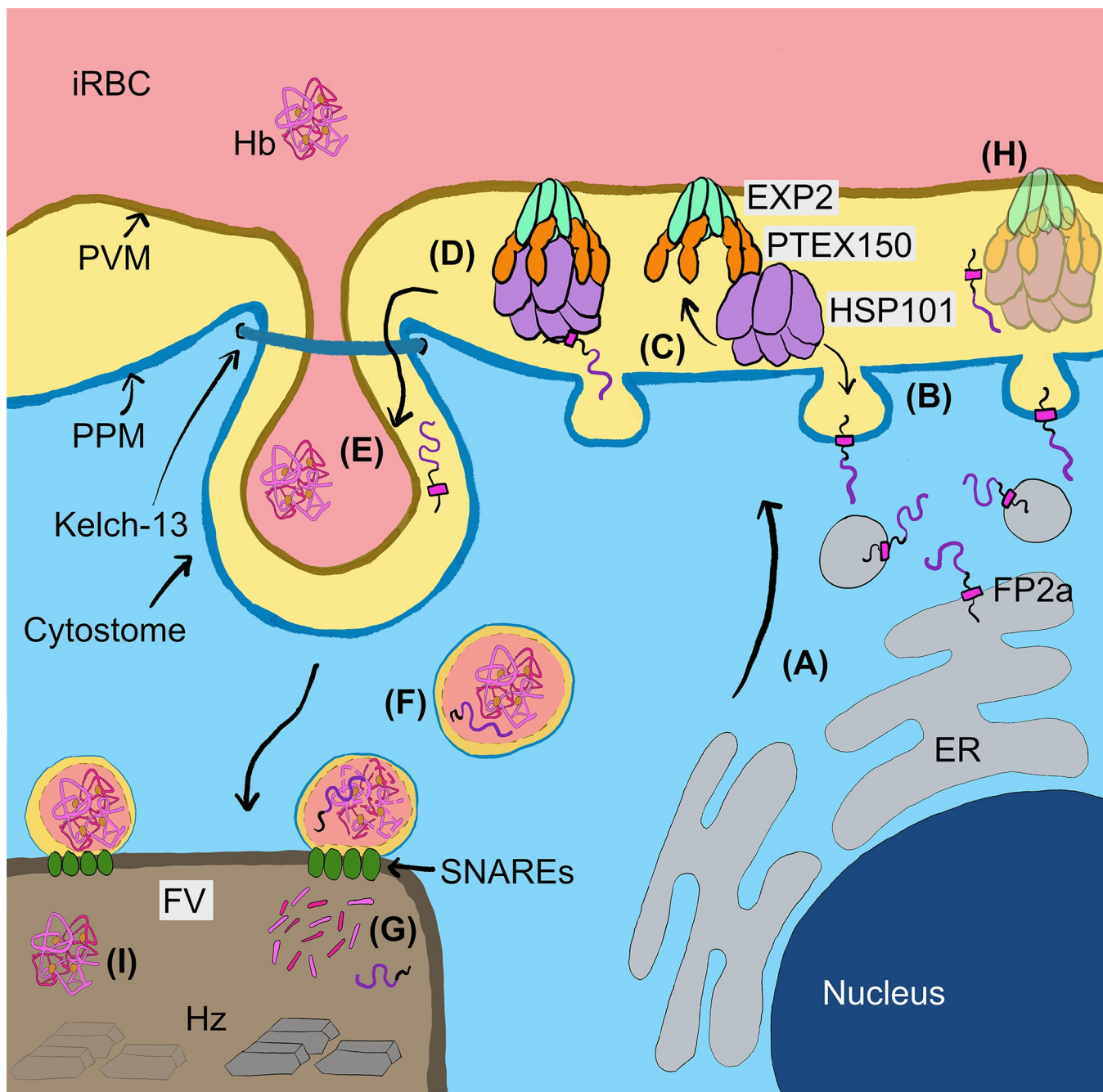


**Fig 8. Model depicting newly identified steps in the FP2a trafficking pathway to the food vacuole.** By integrating the data from this study, we propose a new model for the trafficking of FP2a, and potentially other Hb proteases, to the food vacuole (FV). (A) The FP2a protein enters the secretory pathway and travels from the ER to the PV with the N-terminus facing inside the lumen and C-terminus in parasite cytoplasm. (B) The protein is deposited in the PPM by vesicle fusion (TM domain shown in pink), in an N- to C-terminal direction. (C) HSP101 could help extract FP2a from the PPM and into the PV as proposed for transmembrane domain containing exported proteins and then interact with the rest of PTEX, or (D) all the PTEX core components could participate in FP2a extraction from the PPM. FP2a is then escorted to the cytostome, which likely involves additional sorting in the PV by an unknown mechanism. (E) FP2a is taken up via the cytostome formed by invagination of the PVM and PPM. (F) FP2a is then transported to the FV together with Hb. (G) Inside the FV the Hb is digested into smaller peptides, releasing haem, which is sequestered into haemozoin crystals (Hz). (H) Reduced PTEX expression results in accumulation of Hb inside the FV and reduced levels of haemozoin crystal formation. Figure is partially based on Hb trafficking models provided by [32,39].

<https://doi.org/10.1371/journal.ppat.1011006.g008>

[73]. This suggests that PTEX is not essential for trafficking of PM II [5]. Despite the knockdown of PTEX, some Hb peptides were still produced and haemozoin crystals did form, indicating PTEX might only be required for efficient delivery of Hb proteases to the cytostome. However, given the modest level of knockdown achieved in this study the remaining levels of PTEX expression could be sufficient to sustain protease trafficking and Hb digestion. Although reduction in Hb digestion following PTEX knockdown probably contributes to some growth arrest, the dysregulation of other metabolic pathways might also play a greater role in reducing parasite growth, however, our analysis does not indicate what these other pathways are.

As FP2a has been shown to traffic to the cytostomal vesicles via the parasite periphery [34,35] we investigated if PTEX may associate with the FP2a reporters at the PPM. Here we demonstrated that the FP2a reporters likely need to be unfolded prior to crossing the PPM, like exported proteins containing TM domains [10,62,74]. We showed this by appending an inducibly unfoldable DH domain to the reporters, which in its unfoldable form was more strongly localised to the parasite periphery. Our proteinase K protection assays further indicated the direction of insertion into the PPM likely followed an N- to C-terminal direction. Immunoprecipitation assays additionally showed that PTEX was in contact with the 120 aa and 190 aa FP2a reporters and with the native PM II protein, suggesting PTEX could help extract these proteins into the PV lumen. HSP101 has previously been suggested to facilitate the extraction of TM exported proteins from the PPM [75]. An explanation as to how these proteases are trafficked to the cytostome via PTEX is that they are transferred into the PVM via PTEX, which is anchored to the PVM via EXP2, and then incorporated into the innermost membrane of the cytostomal vesicles.

Although this is an attractive explanation for how PTEX assists the Hb proteases to enter the cytostome, further experiments did not strongly support this scenario and PTEX does not have a lateral gate to facilitate the transfer of proteins to the PVM [9,76,77].

From our data it firstly appears that the Hb proteases are not translocated through PTEX into the PVM since the FP2a reporters containing the DH domain did not co-localise to the PVM loops with EXP2 in the presence of WR99210 as has been shown previously for export-blocked PEXEL-DH reporter proteins [63]. Secondly, the 120 aa FP2a reporter was protected from protease degradation when the iRBC was permeabilised with EQT but not when the PVM was lysed with saponin indicating the protease's short 34 aa N-terminal region upstream of its TM domain was projecting into the PV. The fact that the FP2a reporter was more strongly degraded in the absence of WR99210 indicates that PTEX probably only extracts the reporter as far as the PV and not beyond (Fig 8). If PTEX could capture FP2a reporters and deliver them to the cytostome before translocating them into the cytostome lumen for uptake into vesicles, PTEX would be expected to concentrate at the cytostome, which might appear as one to a few distinct puncta at the parasite periphery [36]. We observed these concentrated puncta for FP2a (S3D Fig) but we never observed a particular concentration of EXP2 overlapping with the cytostomal puncta. Instead, a continuous circle or “necklace of beads” surrounding the parasite was observed as previously reported, sometimes with 1–3 PVM loop extensions in older parasites [4–6,8,11,55,63,78]. This likely indicates that PTEX does not directly deposit Hb proteases into the cytostome, however this should be more extensively investigated with markers for both the cytostome (Kelch 13) and PTEX [79].

Following uptake into the PV the Hb proteases possibly employ signals within their N-terminal pro-sequences to specify cytostome trafficking. This signal is likely present between aa 84 to 105 of FP2a, given that truncation studies on FP2a show that reporter cargoes with <84 aa of the FP2a N-terminus accumulate at the PPM but 95 aa and 105 aa show partial and complete trafficking to the food vacuole, respectively [35]. We also found that the length of the FP2a reporter appears to be important for efficient trafficking to food vacuole as the 190 aa

FP2a reporter trafficked more efficiently than the 120 aa reporter, which could contribute to more efficient PPM extraction.

In conclusion, we propose a new model for Hb protease trafficking involving PTEX where the early acting FP2a, PM II and possibly other Hb proteases of these families are extracted by the PTEX complex from the PPM and into the PV space. The Hb proteases do not appear to be subsequently translocated across the PVM and beyond into the iRBC since the 120 aa FP2a reporter was not detected in the iRBC or within cargo-associated PVM loops (Fig 8). Furthermore, our FP2a reporter did not degrade in the presence of EQT and proteinase K as the exported GBP130 protein did. We therefore propose that HSP101 could bind to the short 34 aa N-terminal section of FP2a that precedes the TM domain and projects into the PV. The HSP101/FP2a complex could then dock with the rest of PTEX, which may activate HSP101 activity to extract the FP2a reporter into the PV (Fig 8). Alternatively, the intact PTEX complex could directly bind the N-terminal region of FP2a reporter and extract the protease into the PV. Thereby, PTEX would help extract the Hb proteases into the PV providing the correct orientation of the proteases for entry into the cytostome. Although our study has not resolved the complete mechanism of protease transfer into the Hb containing cytostomal vesicles, it could serve as a future starting point to better understand this important process.

## Material and methods

### Cloning

The *fp2a* gene was appended with a single HA-tag followed by a *glmS* before the 3' stop codon using CRISPR/Cas9. The construct was designed using a multi-step PCR where DNA fragments were amplified from 3D7 WT parasite genomic DNA and the tagging sequence (HA*glmS*) and then joined together through subsequent amplification using the outermost primer pairs as shown in detail in S3A Fig. The PM II-mScarlet was designed the same way, where the HA*glmS* was exchanged for the mScarlet tag (S15A Fig). Flanks were then ligated into a pBSK Bluescript plasmid (Stratagene) and 50 µg of DNA was co-transfected into 3D7 WT (FP2a) or PTEX150-HA*glmS* (PM II-mScarlet) parasites with 50 µg of a Cas9 expressing plasmid (pCas9) [80]. In the Cas9 plasmid, the guide RNA sequence was under the regulation by a U6 RNA promoter and the plasmid also contained the human dehydrofolate reductase (hDHFR) cassette to confer resistance to WR99210 [80]. Relevant single guide RNA (sgRNA) oligonucleotides were chosen based on the list published by Ribeiro *et al.* 2018 [81]. Single guide RNAs were mixed together by adding 1 µL sgRNA forward primer (100 µM stock), 1 µL sgRNA reverse primer, 1 µL 10x T4 DNA ligase (Thermo Fisher), 0.5 µL T4 Polynucleotide kinase (Thermo Fisher) and 6.5 µL water and annealed in a thermocycler (37°C for 30 min, 94°C for 5 min and then ramped down to 25°C at 5°C per min). The annealed guide RNAs were then ligated into the Cas9 plasmid, which was pre-cut with *BbsI* enzyme. A mutated version of the Cas9 plasmid (mpCas9) was prepared for PM II-mScarlet, where the hDHFR was exchanged for a Blasticidin S Deaminase (BSD) drug selection marker since the PTEX150-HA*glmS* line was already WR99210-resistant. The BSD coding sequence from pEF-Hyp1-N-luc-DH-APEX [63] was amplified in two overlapping fragments so that an internal *BbsI* site could be synonymously mutated to prevent unwanted cleavage prior to insertion of the guide RNA. The first BSD fragment was amplified with BSD\_NcoF and *BbsI*\_MutR and the second BSD fragment was amplified with *BbsI*\_MutF and BSD\_SacIIR under standard conditions. PCR fragments were then joined together with *BbsI*\_MutF and BSD\_SacIIR and the full-size BSD coding sequence was excised with *NcoI* and *SacII* and ligated into similarly digested pCas9. The pCas9 was selected for by WR99210 (Jacobs Pharmaceutical) or mpCas9 with Blasticidin S (Life technologies) for 7 days and genomic DNA extracted when transgenic parasites

were obtained to confirm correct integration of epitope tag to gene of interest using PCR. All primers and DNA sequences are listed in [S2 Table](#).

The previously published plasmid pEF-Hyp1-Nluc-DH [55] was used to generate the three different FP2a constructs, pFP2a 120/FP2a 190/FP2a NT-Nluc-DH-FL ([Fig 3A](#)). The Hyp1 region of the reporter was removed by excision with *Xba*I and *Nco*I and replaced with the relevant FP2a sequence. FP2a 120 aa and 190 aa contained the first 120/190 aa from the FP2a gene. To generate the FP2a NT, a forward primer was designed after the TM (after aa 57 of the FP2a sequence) and coupled with the reverse primer created for the 190 aa construct giving an ~120 aa sequence. Plasmids were transfected into the HSP101-HAglmS parasite line and expressed episomally under Blasticidin S selection. Primers are listed in [S2 Table](#).

### Parasite culturing

Continuous culture of *P. falciparum* was maintained at 4% haematocrit in human RBCs in AlbumaxII media (RPMI-1640, 25 mM HEPES, 367 μM hypoxanthine, 31.25 μg/mL Gentamicin, 0.5% AlbumaxII and 25 mM NaHCO<sub>3</sub>) and kept at 37°C in gas chambers (1% O<sub>2</sub>, 5% CO<sub>2</sub> and 96% N<sub>2</sub>). Method adapted from Trager and Jensen [82].

### Immunofluorescence assays

For WR99210 trapping experiments, parasite culture was treated with 100 μg/mL heparin (Sigma-Aldrich) to prevent parasite invasion [83] and late schizont stages purified using a 67% percoll (Cytiva) gradient, where the percoll was diluted in PBS and RPMI-1640 media. Heparin was then washed off and parasites allowed to invade for 4 h and then treated in 5% sorbitol for 10 min at 37°C to remove any remaining schizonts. Ring stage parasites were then treated ± 10 nM WR99210. For BFA assays, parasites were synchronised in 5% sorbitol (Sigma-Aldrich) for 10 min at 37°C. Late ring/early trophozoite stage parasites (20 to 24-hpi) were then treated with 18 μM BFA made up in DMSO or 0.001% DMSO for 5 h and then culture harvested for IFA. For haemozoin crystal and saponin lysis experiments, 3D7 WT, PTEX150-HAglmS, HSP101-HAglmS and FP2a-HAglmS parasite lines were sorbitol synchronised at ring stage (~12 to 16-hpi) and treated ± 2.5 mM GlcN (haemozoin crystal) or ± 1 mM GlcN (saponin) and 100 μg/mL heparin at trophozoite stage to prevent parasite invasion or with 30 nM ML10 which prevents parasite egress [84]. At late schizont stage (segmented), drugs were washed off (either heparin or ML10) and parasites given 4 h to invade uninfected RBCs as described above and then lysed in 5% sorbitol to remove any remaining schizonts. Cells were then harvested the next cell cycle at late ring stage/early trophozoite stage (20 to 24-hpi) for IFA. For heparin treated parasites, percoll density gradient was used to purify schizonts parasites prior to invasion.

For all assays, parasite culture was diluted in PBS and mounted on Poly-L-Lysine (Sigma-Aldrich) treated coverslips, fixed in 4% paraformaldehyde/ 0.0075% glutaraldehyde in PBS for 20 min and permeabilised in 0.1% TX-100 with 0.1 M glycine diluted in PBS for 15 min as previously described [85,86]. Samples were blocked for 1 h in 3% bovine serum albumin (Sigma-Aldrich) and subsequently incubated in primary antibodies (overnight) and secondary antibodies (1 h) with 3x washes of 0.02% TX-100 (in PBS) in-between. Coverslips were mounted on slides containing mounting media with DAPI (Vectashield) and sealed with nail polish. For the saponin lysis experiment, cells were incubated with ice-cold 0.05% saponin (diluted in PBS) on ice for 10 min, pelleted at 50 g for 3 min and washed 3x in 500 μL PBS. Cells were then fixed and probed with antibodies as described above. Images were visualised using the Zeiss Axio Observer Z1 inverted widefield microscope and processed using Image J software. List of antibodies can be found in [S3 Table](#).

Pearson's correlation coefficients were used to determine co-localisation of Nluc and EXP2. Images were acquired with identical exposure settings and analysis completed on raw images using Fiji software with JACoP plugin. For the saponin lysis experiment, exposure settings were the same for the fluorescent channel of interest for all cells ( $\pm$  GlcN) for direct comparison of signal intensity using raw images. To measure signal only within the parasite, an area was manually drawn around the parasite using the EXP2 signal (PVM) for guidance. To quantify the signal, the mean fluorescence intensity for the Hb channel was measured using Image J software and the signal corrected by subtracting the background mean fluorescent signal. Background mean was measured for each field of view used for the analysis, where the average signal of three background areas was subtracted from the cells analysed within the same field of view. For haemozoin crystal experiments, the area was calculated as described for saponin lysis experiments using the DIC channel for guidance and crystals counted as "present" or "absent" completed by two individual counters. All statistical analysis was completed using GraphPad 8 Prism software using Student's t test with Welch correction. Number of cells analysed and replicates are indicated within each figure.

### Live cell imaging

Heparin synchronised parasite culture with a 4-h invasion window was diluted in media 1:1 at late ring stage (~20-hpi) and evenly distributed over a glass slide and a coverslip placed on top and sealed with wax. Cells were visualised by microscopy as described for IFAs. Analysis was done using Image J where the mScarlet signal was categorised into either 'dot' inside the parasite or 'crescent/circle' at the parasite periphery by looking at the DIC channel and the Cy3 channel. Three individual counters completed categorisation of cells. Number of cells analysed and replicates are indicated within figure.

### Growth assays

Sorbitol synchronised trophozoite stage parasite culture (~24 to 28-hpi) was adjusted to 1% haematocrit and 0.3% parasitemia and treated with 0, 0.15 or 1 mM GlcN and subsequently plated in 100  $\mu$ L aliquots on 96-well plates in technical triplicate. Parasite culture was harvested at trophozoite stage in each cell cycle, for three consecutive cell cycles and stored at -80°C until all time points had been collected. LDH was then measured as a proxy for parasite growth as previously described [52,53], where 30  $\mu$ L of parasite culture was resuspended with 75  $\mu$ L of LDH reagent (0.083 M Tris, 185 mM lactic acid [adjusted to pH 7.5], 0.17% TX-100, 0.83 mM acetylpyridine adenine dinucleotide, 0.17 mg/mL Nitroblue tetrazolium, 0.08 mg/mL phenazine ethosulphate). Plates were incubated in the dark for 45 min and absorbance measured at 650 nm. Growth was normalised to time point zero (assay set up) and 0 mM GlcN set as 100% growth for each cycle. Statistical analysis was done using Student's t test with Welch correction in GraphPad Prism 8 for 2 biological replicates. For Giemsa-stained smear assays, parasite culture was treated with increasing concentration of GlcN at trophozoite stage (~24 to 28-hpi) and given 30 nM ML10 to prevent parasite egress. Parasites were given 4-h invasion window and harvested at 18-hpi, 24-hpi and 30-hpi.

### Western blot

For Hb build-up knockdown experiments, heparin or ML10 synchronised (4-h invasion window) trophozoite stage parasites were treated for one cell cycle (trophozoite to trophozoite) with increasing concentrations of GlcN (Sigma-Aldrich). For FP2a reporter expression experiments, heparin (4-h invasion window) synchronised parasites were prepared and harvested at 4 different time points, 24-, 28-, 32- and 36-h after invasion window. For other experiments,

parasites were sorbitol synchronised at ring stage (~12 to 16-hpi). When harvesting parasites for western blot, trophozoite stage parasites were lysed in 0.09% saponin in PBS containing protease inhibitor cocktail (Roche) on ice for 10 min. For the Hb build-up experiments, parasite pellet was extensively washed in PBS containing protease inhibitor cocktail after saponin lysis to remove residual Hb. For all experiments unless otherwise mentioned, parasite pellets were diluted in 1x sample buffer (6x: 0.3 M Tris, 60% v/v glycerol, 12 mM EDTA, 12% SDS, 0.05% bromophenol blue), sonicated 3x cycles (Bioruptor pico, 30 sec on/30 sec off) and reduced in 100 mM dithiothreitol (DTT) prior to fractionation on 3–12% Bis-Tris gels (Invitrogen). Proteins were transferred to nitrocellulose membranes (iBlot, 20 V, 7 min), blocked in 1% casein in PBS for 1 h and incubated in primary antibodies ([S3 Table](#)) overnight and in secondary antibodies for 1 h (Invitrogen) in the dark. For chemiluminescence detection of chicken anti-FLAG and rat anti-RFP (to detect mScarlet), membrane was additionally incubated for 5 min in SuperSignal substrate (Pierce). Blots were visualised and densitometry analysis performed using Image Studio (LI-COR). Graphs and statistical analysis, Student's t test with Welch correction or simple linear regression, were completed using GraphPad 8 Prism Software. Image Studio was also used to measure the length of the FP2a 120 aa reporter in the proteinase K protection assay, where the molecular marker was used to estimate the shift in size.

### Co-immunoprecipitation assays

Sorbitol synchronised ring stage parasites (~12 to 16-hpi) were treated  $\pm$  10 nM WR99210 for ~16 h and subsequently harvested at trophozoite stage (~28–32-hpi) via magnet purification (LS columns, Militeyni). The iRBC pellet was resuspended in 20x pellet volume of 1x modified radioimmunoprecipitation (RIPA) buffer (1% TX-100, 0.1% SDS, 10 mM Tris [adjusted to pH 7.5], 150 mM NaCl) [62] containing protease inhibitor cocktail. Cells were lysed via 2x cycles of freeze/thawing, pelleted at 16,000 g for 10 min at 4°C and resultant supernatant was transferred to a new tube. Two different methods were used, either HA or IgG IP assays:

1. For HA IP assays, 250  $\mu$ L of supernatant (~2.5 mg of protein) was diluted in 750  $\mu$ L of lysis buffer and 50  $\mu$ L of diluted supernatant transferred to a new tube and used as assay input. Diluted supernatant was incubated overnight with 50  $\mu$ L of pre-washed 50/50 anti-HA agarose bead slurry (Sigma-Aldrich, diluted in lysis buffer)
2. For IgG IP assays, 200  $\mu$ L of supernatant (2 mg of protein) was diluted in lysis buffer to make 1 mL total volume and 50  $\mu$ L of diluted supernatant transferred to a new tube and used as assay input. The diluted supernatant was incubated with IgG overnight. The next day, IgG assay samples were incubated with 100  $\mu$ L of pre-washed 50/50 Protein Sepharose A slurry (Sigma-Aldrich, diluted in lysis buffer) for 1 h. Samples for both HA and IgG assays were then passed through a Micro-Bio spin column (Bio-Rad) and eluted in 50  $\mu$ L 1x sample buffer for 5 min at room temperature. Input was resuspended in 10  $\mu$ L of 6x sample buffer and both input and elution were reduced (HA IP) by addition of 100 mM DTT or kept non-reduced (IgG IPs) prior to SDS-PAGE and western blot.

### Proteinase K protection assay

Sorbitol synchronized ring stage parasites (~12 to 16-hpi) were treated  $\pm$  10 nM WR99210 and enriched via magnet purification at trophozoite stage parasites (~24 to 28-hpi). Parasite pellet was used immediately for proteinase K protection assays as previously described [87] but with a few modifications. 20  $\mu$ L of the iRBC pellet was resuspended in 80  $\mu$ L of PBS + protease inhibitors cocktail supplemented with 1.6  $\mu$ g of recombinant EQT (made in-house) and

incubated for 10 min at 37°C. Samples were centrifuged at 1,000 g for 3 min at 4°C and supernatant transferred to a new tube and kept on ice. The pellet was subsequently washed 3x in PBS and divided equally between four tubes. Samples were pelleted and supernatant discarded. 100 µL PBS was added to tube 1, 100 µL PBS + proteinase K (20 µg) to tube 2, 100 µL 0.03% saponin in PBS + proteinase K to tube 3 and 100 µL of 0.25% v/v TX-100 in PBS + proteinase K to tube 4. All tubes were incubated on ice for 30 min. To stop the proteinase K activity and precipitate proteins, 11.1 µL of trichloroacetic acid was added to each tube, resuspended thoroughly and incubated on ice for 10 min. Samples were centrifuged at 16,000 g for 20 min at 4°C. Supernatant was discarded and 500 µL of 100% ice-cold acetone was added to the pellet and centrifuged at 16,000 g for 10 min at 4°C. Supernatant was discarded and pellet left to air-dry. The dried pellet was resuspended in 100 µL of 1x sample buffer, and 26 µL of 4x sample buffer was added to EQT supernatant. All samples were reduced in 100 mM DTT and prepared for western blot.

### Metabolite extraction and analysis

Sorbitol synchronised parasite culture with ~10% trophozoite stage parasites (~24 to 28-hpi) were treated with 0, 0.15 or 1 mM GlcN plus heparin (100 µg/mL) to prevent parasite invasion. At late schizont stage the heparin was removed and parasite culture concentrated to 8% haematocrit and left shaking (85 RPM) at 37°C for 4 h to allow parasites to invade new RBCs. Culture was then sorbitol synchronised and parasite pellet placed back into culture at 1% haematocrit at 37°C. GlcN concentration was maintained throughout all steps, except during sorbitol treatment. PTEX150-HAglmS parasite culture was harvested at 18, 24 and 30-hpi or at a single time point 24-hpi including additional 3D7 WT control. For metabolite extraction, samples were prepared in three technical replicates, each replicate containing 1 mL warm media and 1x10<sup>8</sup> cells. All 12 tubes (0, 0.15, 1 mM GlcN and uRBCs) were incubated at 37°C. Technical triplicates were processed together for the following steps at 4°C. Samples were centrifuged at 12,000 g for 30 s, supernatant removed and pellet resuspended in 1 mL ice-cold PBS. Samples were centrifuged as before and final pellet was resuspended in 200 µL of 80% acetonitrile (in water). The samples were centrifuged at 18,000 g for 5 min, supernatant transferred to fresh tubes and stored at -80°C until processed by mass spectrometry as previously described [88].

Polar metabolite detection was performed on an Agilent 6550 Q-TOF mass spectrometer operating in negative mode. Metabolites were separated on a SeQuant ZIC-pHILIC column (5 µM, 150 X 4.6 mm, Millipore) using a binary gradient with a 1,200 series HPLC system across a 45 min method using 20 mM ammonium carbonate (pH 9) and acetonitrile, as described previously [88]. The scan range was 25–1,200 m/z between 5 and 30 min at 0.9 spectra/s. An internal reference ion solution was continually run (isocratic pump at 0.2 mL/min) throughout the chromatographic separation to maintain mass accuracy. Other liquid chromatography parameters were: autosampler temperature 4°C, injection volume 5–10 µL and data was collected in centroid mode with Mass Hunter Workstation software (Agilent). Raw Agilent.d files were converted to mzXML with MSconvert and analysed using the Maven software package [89]. Following alignment, metabolite identification was performed either with exact mass (<10 ppm) or retention time matching to authentic standards (approximately 150 in-house metabolite standards).

### Supporting information

**S1 Fig. Metabolite heat maps.** (A) Heat map corresponding to [S1 Table](#) for PTEX150-HAglmS metabolomics time course (18, 24, 30-hpi) experiment. (B) Heat map corresponding

to [S1 Table](#) for 3D7 and PTEX150-HAglmS metabolomics experiment. Numbers represent metabolites listed in [S1 Table](#), where Hb peptides have been highlighted in bold. Fold change for both heat maps was calculated using the following formula, Fold change =  $\log_2$  (GlcN treated / untreated).

(TIF)

**S2 Fig. Giemsa smears for 3D7 WT and PTEX150-HAglmS after GlcN treatment.** 3D7 WT and PTEX150-HAglmS parasites were treated with increasing concentration of GlcN at trophozoite stage (T = 0). Parasites were given 4-h invasion window and then blood smears were taken at 18-hpi, 24-hpi and 30-hpi. Figures are representative images from 3 biological replicates, where red box around images in 24-hpi and 30-hpi emphasize growth stall observed, this was more prominent in 2.5 mM GlcN treatment. Arrows point to expansion of the food vacuole, which was sometimes observed.

(TIF)

**S3 Fig. Generation and characterisation of the FP2a-HAglmS parasite line.** (A) i) CRISPR-Cas9 was used to append the *fp2a* gene with a HA tag and a *glmS* riboswitch. ii) This was done in a multi-step PCR, where primer 1F (forward) was located ~500 bases upstream from the gene stop codon and primer 2R (reverse) started at the gRNA cut site, where 4 shield mutations were added to the end of the primer. Primer 3F overlapped with primer 2R and had the 4 shield mutations at the start of the primer and 4R was located just before the stop codon and included the first few bases of the HA tag. The HAglmS tag was amplified using the HA\_F and glmS\_R primers. The 3'UTR was amplified using 5F primer, which had the last few bases of *glmS* at the start and the 6R primer started ~500 bp downstream from the stop codon. These 4 PCRs were then joined together. iii) The flank was ligated into the pBSK vector and transfected together with the iv) Cas9 plasmid containing the gRNA. v) When transgenic parasites were obtained, genomic DNA was extracted and PCR completed to confirm correct integration of the HAglmS tag into the target gene, where F\_Int was located upstream of F1. (B) PCR was used to confirm the correct integration of the tag to the target gene, where 3D7 WT was used as a negative control for integration. The position of PCR primers used to confirm integration are shown in panel A, where FInt, is the forward PCR integration primer. F, forward primer. glmS\_R, reverse primer. (C) Correct size and level of FP2a knockdown was confirmed using western blot. >90% of FP2a was knocked down after one cell cycle of GlcN treatment. P stands for pro FP2a and M stands for mature FP2a. The HA-tag adds approximately 3 kDa to the target protein. The mark on the right-hand side of the blot is an artefact. Mouse anti-HA detects FP2a-HA and rabbit anti-HSP70-1 was used as a loading control. Blot is representative of 3 biological replicates. Full-length blots are shown in [S16 Fig](#). (D) Immunofluorescence assays where mouse anti-HA detects target protein and rabbit anti-EXP2 was used as a PVM marker. The images indicate that FP2a displays diffuse localisation in the parasite cytoplasm, sometimes with a concentrated puncta at the parasite periphery, likely representing the cytostome (white arrows). The HA antibody signal against FP2a-HA partly overlaps with rabbit anti-CRT which labels the food vacuole membranes. Food vacuole lumen, indicated by the dark haemoglozin crystals in the DIC images, are not well labelled for FP2a-HA likely due to the HA epitope tag being proteolytically degraded in the food vacuole. Scale bars = 5  $\mu$ m. (E) Multi-cycle LDH growth assays were performed over 3 consecutive cell cycles. No significant growth defect was observed for FP2a (T = 1, 0.5 mM GlcN P = 0.6657 and 1 mM GlcN P = 0.8992, T = 2, 0.5 mM GlcN P = 0.5196 and 1 mM GlcN P = 0.0756, T = 3, 1 mM GlcN P = 0.0649) or 3D7 WT (T = 1, 0.5 mM GlcN P = 0.9961 and 1 mM GlcN P = 0.1011, T = 2, 0.5 mM GlcN P = 0.3998, T = 3, 0.05 mM GlcN P = 0.77 and 1 mM GlcN P = 0.2653) when treated with different concentrations of GlcN except for 3D7 WT 1 mM GlcN condition in the second cycle of treatment

( $P = 0.0324$ ) and FP2a-HAglmS 0.5 mM GlcN condition in the third cycle of treatment ( $P = 0.0173$ ). Statistics were completed using Student's t test with Welch correction. Graphs show 2 biological replicates completed in technical triplicate. Error bars = SD. Data for each parasite line was normalised to 0 GlcN treatment for each time point.

(TIF)

**S4 Fig. Giemsa smears for HSP101-HAglmS and FP2a-HAglmS parasite lines after GlcN treatment.** HSP101-HAglmS and FP2a-HAglmS parasites were treated with increasing concentration of GlcN at trophozoite stage ( $T = 0$ ). Parasites were given 4-h invasion window and then blood smears were taken at 24-hpi. Figures are representative images from 3 biological replicates, where red box around images emphasize growth stall observed, this was more prominent in 2.5 mM GlcN treatment. Arrows point to expansion of the food vacuole, which was sometimes observed.

(TIF)

**S5 Fig. Full-length western blots for Fig 2.**

(TIF)

**S6 Fig. Knockdown of PTEX150-HAglmS and HSP101-HAglmS results in build-up of full-length Hb inside the parasite and reduced haemozoin crystal formation.** (A) Simple linear regression analysis was performed on protein expression and Hb build-up from western blots presented in Fig 2B for PTEX150-HAglmS, HSP101-HAglmS and FP2a-HAglmS. All parasite lines showed significant regression slope, where  $P$  values are shown in each graph along with  $R^2$ . The blue dots on the x-axis are  $\log_{10}$  of mean of the fold difference in protein expression for 6 biological replicates for 0.15 and 1 mM GlcN and 3 biological replicates for 2.5 mM GlcN plotted against  $\log_2$  of the fold difference for individual biological replicates for Hb build-up (y-axis). The SD for the x-axis shown is as follows, PTEX150-HAglmS ( $X = 2$ , SD = 0;  $X = 1.82$ , SD = 0.06,  $X = 1.75$ , SD = 0.12,  $X = 1.67$ , SD = 0.21), HSP101-HAglmS ( $X = 2$ , SD = 0;  $X = 1.73$ , SD = 0.14,  $X = 1.69$ , SD = 0.08,  $X = 1.71$ , SD = 0.21), FP2a-HAglmS ( $X = 2$ , SD = 0;  $X = 0.99$ , SD = 0.19;  $X = 0.71$ , SD = 0.52,  $X = 0.74$ , SD = 0.61). (B) Highly-synchronous 3D7 WT, PTEX150-HAglmS, HSP101-HAglmS and FP2a-HAglmS trophozoite stage parasites were treated  $\pm$  2.5 mM GlcN for one cell cycle and harvested for IFA. Haemozoin crystals in the DIC channel were counted (present or absent). Images are representative of 3 (3D7 WT, PTEX150-HAglmS, FP2a-HAglmS) or 2 (HSP101-HAglmS) biological replicates. (C) Both PTEX150-HAglmS and HSP101-HAglmS knockdown experiments shown in panel B resulted in significantly less crystal formation compared to untreated cells when using Student's t test with Welch correction. No significant difference in haemozoin crystal count was observed for 3D7 WT or FP2a-HAglmS parasites, although FP2a-HAglmS parasites often appeared to have smaller crystals. (\*) Indicates  $P = 0.0247$  (PTEX150-HAglmS) and  $P = 0.0277$  (HSP101-HAglmS). Error bars = SD from 2 individuals counting. (D) Area of the parasites analysed in panel C (completed as described in Fig 2E) showed significant difference in size for GlcN treated PTEX150-HAglmS parasites compared with untreated indicating parasite growth was affected but no significant difference was observed for HSP101-HAglmS knockdown for the cells used in the analysis. Middle line represents mean and error bars = SD. (\*\*\*\*) Indicates  $P < 0.0001$ . Each dot on the graph represents one cell analysed. (E) FP2a-HAglmS parasites sometimes showed expansion of the food vacuole as previously observed in Giemsa-stained smears (S4 Fig), indicated with an arrow. When stained with rabbit anti-human haemoglobin antibody, a build-up of Hb was observed inside the food vacuole as previously observed in IFA treated with saponin (Fig 2C).

(TIF)

**S7 Fig. Full-length western blots for Fig 3B.**  
(TIF)

**S8 Fig. Additional images for FP2a reporter trapping shown in Fig 4.**  
(TIF)

**S9 Fig. Western blot time course indicates that the 120 and 190 aa FP2a reporters are expressed similarly from 24 to 40-hpi while the NT reporter is degraded as the parasite matures.** Synchronous (4-h invasion window) parasite cultures for the three FP2a reporter lines were divided in four and harvested via saponin lysis at four sequential time points: 24 to 28-hpi, 28 to 32-hpi, 32 to 36-hpi and 36 to 40-hpi. Chicken anti-FLAG and rabbit anti-Nluc were used to visualise the FP2a reporters, mouse anti-HA to visualise the HSP101-HAglmS (parental line) and rabbit anti-HSP70-1 was used as a loading control. The expected size of each reporter is indicated with (\*), where the cleavage of Nluc from the 120 and 190 aa reporters was observed in each time point (lanes 2, 3, 5, 6, 8, 9, 11 and 12), likely due to cleavage upon entry into the food vacuole. This cleavage of Nluc was not observed for the NT reporter (lanes 1, 4, 7 and 10), which does not enter the food vacuole. The NT reporter was also degraded more, and the expression of the full-length reporter diminishes as the parasite matures (lanes 1 and 4 vs. lanes 7 and 10), whilst expression of the 120 and 190 aa reporters remains stable across each time point. These data indicate that the optimal time point to study these three reporters was in the range of 24 to 32-hpi, as indicated in bold. This blot represents 2 biological replicates. Full-length blots are shown in [S17 Fig](#).  
(TIF)

**S10 Fig. Full-length western blots for Fig 5A.**  
(TIF)

**S11 Fig. The 120 aa and the 190 aa FP2a reporters interact with PTEX150 and EXP2.** Immunoprecipitation assays with parasites treated with  $\pm$  10 nM WR99210 were completed on the four reporter lines using Protein Sepharose A where (A) PTEX150 or (B) EXP2 protein specific antibodies were incubated with parasite lysate to Co-IP interacting proteins. Both 120 aa (line 13) and 190 aa (line 15) showed stronger association with (A) PTEX150 and (B) EXP2 in-WR99210 treatment as determined by densitometry ([S12 Fig](#)). The Hyp1 reporter showed reverse association to FP2a reporters and NT showed some background signal in both conditions. (A) PTEX150 and (B) EXP2 both co-precipitated with other PTEX components (lanes 9–16). Chicken anti-FLAG was used to probe for the reporter, mouse anti-HA for HSP101-HAglmS and rabbit 741 for PTEX150. Both (A) and (B) blots represent 3 biological replicates. The asterisks indicate stronger signal when comparing the  $\pm$  WR99210 treatment for respective reporter measured by densitometry of 3 biological replicates. Full-length blots are shown in [S18–S21 Figs](#).  
(TIF)

**S12 Fig. Densitometry measurements for PTEX150 and EXP2 IPs.** (A) The interaction of reporters with PTEX150 (r942) and EXP2 (r1167) presented in [S11 Fig](#) A was graphed, where FLAG elution was adjusted to input. Each dot represents 1 biological replicate. (B) The interaction of reporters with PTEX150 (r942) and EXP2 (r1167), where the fold difference of the FLAG elution/input was adjusted to untreated (- WR99210). Error bars = SD from 3 biological replicates.  
(TIF)

**S13 Fig. Full-length western blots for Fig 6A.**  
(TIF)

**S14 Fig. Full-length western blots for Fig 7E.**

(TIF)

**S15 Fig. Establishment of PM II mScarlet in a PTEX150-HAglmS background.** (A) The *pm ii* gene was C-terminally tagged with mScarlet as described for FP2a in [S2 Fig A](#) and introduced into a PTEX150-HAglmS background. The primers used to amplify the mScarlet tag were the same as for the HAglmS tag and all fragment joined together as explained for FP2a-HAglmS. (B) Correct integration of mScarlet to PM II was confirmed via PCR, where genotyping primers are displayed in panel A.

(TIF)

**S16 Fig. Full-length western blots for S3C Fig.**

(TIF)

**S17 Fig. Full-length western blots for S9 Fig.**

(TIF)

**S18 Fig. Full-length western blots for S11A Fig, part 1.**

(TIF)

**S19 Fig. Full-length western blots for S11A Fig, part 2.**

(TIF)

**S20 Fig. Full-length western blots for S11B Fig, part 1.**

(TIF)

**S21 Fig. Full-length western blots for S11B Fig, part 2.**

(TIF)

**S1 Table. Metabolomics analysis.**

(XLSX)

**S2 Table. List of primers and DNA sequences.**

(DOCX)

**S3 Table. List of antibodies.**

(DOCX)

## Acknowledgments

We thank the Australian Red Cross for the human RBCs used in this study, Jacobus Pharmaceutical for providing the WR99210 and LifeArc for provision of ML10. We thank Cat Nie for technical assistance with troubleshooting of the initial metabolomics experiment, analysis and sample preparation. We thank Paul R. Sanders for technical assistance during the preliminary work of this project. We also thank Leann Tilley and Matthew Dixon for gifting the CRT, ERC and GAPDH antibodies and the Malaria Experimental Genetics 2018 course for providing the pCas9 plasmid.

## Author Contributions

**Conceptualization:** Thorey K. Jonsdottir, Brendan Elsworth, Brendan S. Crabb, Paul R. Gilson.

**Formal analysis:** Thorey K. Jonsdottir, Simon Cobbold, Mikha Gabriela.

**Funding acquisition:** Brendan S. Crabb, Paul R. Gilson.

**Investigation:** Thorey K. Jonsdottir, Brendan Elsworth, Simon Cobbolt, Mikha Gabriela, Ellen Ploeger, Molly Parkyn Schneider, Sarah C. Charnaud, Madeline G. Dans, Hayley E. Bullen, Paul R. Gilson.

**Methodology:** Thorey K. Jonsdottir, Simon Cobbolt, Mikha Gabriela.

**Project administration:** Thorey K. Jonsdottir, Hayley E. Bullen, Paul R. Gilson.

**Resources:** Malcolm McConville, Brendan S. Crabb, Paul R. Gilson.

**Supervision:** Sarah C. Charnaud, Hayley E. Bullen, Brendan S. Crabb, Paul R. Gilson.

**Validation:** Thorey K. Jonsdottir, Mikha Gabriela.

**Visualization:** Thorey K. Jonsdottir.

**Writing – original draft:** Thorey K. Jonsdottir, Simon Cobbolt, Hayley E. Bullen, Paul R. Gilson.

**Writing – review & editing:** Thorey K. Jonsdottir, Simon Cobbolt, Hayley E. Bullen, Paul R. Gilson.

## References

1. W.H.O. World Malaria Report 2022. Geneva: World Health Organisation; 2022.
2. Milner DA, Jr. Malaria Pathogenesis. *Cold Spring Harb Perspect Med*. 2018; 8(1):a025569. <https://doi.org/10.1101/cshperspect.a025569> PMID: 28533315
3. Marti M, Spielmann T. Protein export in malaria parasites: many membranes to cross. *Curr Opin Microbiol*. 2013; 16(4):445–51. <https://doi.org/10.1016/j.mib.2013.04.010> PMID: 23725671
4. de Koning-Ward TF, Gilson PR, Boddey JA, Rug M, Smith BJ, Papenfuss AT, et al. A newly discovered protein export machine in malaria parasites. *Nature*. 2009; 459(7249):945–9. <https://doi.org/10.1038/nature08104> PMID: 19536257
5. Beck JR, Muralidharan V, Oksman A, Goldberg DE. PTEX component HSP101 mediates export of diverse malaria effectors into host erythrocytes. *Nature*. 2014; 511(7511):592–5. <https://doi.org/10.1038/nature13574> PMID: 25043010
6. Elsworth B, Matthews K, Nie CQ, Kalanon M, Charnaud SC, Sanders PR, et al. PTEX is an essential nexus for protein export in malaria parasites. *Nature*. 2014; 511(7511):587–91. <https://doi.org/10.1038/nature13555> PMID: 25043043
7. Charnaud SC, Kumarasingha R, Bullen HE, Crabb BS, Gilson PR. Knockdown of the translocon protein EXP2 in *Plasmodium falciparum* reduces growth and protein export. *PLoS One*. 2018; 13(11):e0204785. <https://doi.org/10.1371/journal.pone.0204785> PMID: 30439948
8. Bullen HE, Charnaud SC, Kalanon M, Riglar DT, Dekiwadia C, Kangwanrangsang N, et al. Biosynthesis, localization, and macromolecular arrangement of the *Plasmodium falciparum* translocon of exported proteins (PTEX). *J Biol Chem*. 2012; 287(11):7871–84. <https://doi.org/10.1074/jbc.M111.328591> PMID: 22253438
9. Ho CM, Beck JR, Lai M, Cui Y, Goldberg DE, Egea PF, et al. Malaria parasite translocon structure and mechanism of effector export. *Nature*. 2018; 561(7721):70–5. <https://doi.org/10.1038/s41586-018-0469-4> PMID: 30150771
10. Matthews KM, Kalanon M, de Koning-Ward TF. Uncoupling the threading and unfoldase actions of *Plasmodium* HSP101 reveals differences in export between soluble and insoluble proteins. *mBio*. 2019; 10(3). <https://doi.org/10.1128/mBio.01106-19> PMID: 31164473
11. Garten M, Nasamu AS, Niles JC, Zimmerberg J, Goldberg DE, Beck JR. EXP2 is a nutrient-permeable channel in the vacuolar membrane of *Plasmodium* and is essential for protein export via PTEX. *Nat Microbiol*. 2018; 3(10):1090–8. <https://doi.org/10.1038/s41564-018-0222-7> PMID: 30150733
12. Matthews K, Kalanon M, Chisholm SA, Sturm A, Goodman CD, Dixon MW, et al. The *Plasmodium* translocon of exported proteins (PTEX) component thioredoxin-2 is important for maintaining normal blood-stage growth. *Mol Microbiol*. 2013; 89(6):1167–86. <https://doi.org/10.1111/mmi.12334> PMID: 23869529

13. Matz JM, Matuschewski K, Kooij TW. Two putative protein export regulators promote *Plasmodium* blood stage development *in vivo*. *Mol Biochem Parasitol*. 2013; 191(1):44–52.
14. van Ooij C, Tamez P, Bhattacharjee S, Hiller NL, Harrison T, Liolios K, et al. The malaria secretome: from algorithms to essential function in blood stage infection. *PLoS Pathog*. 2008; 4(6):e1000084. <https://doi.org/10.1371/journal.ppat.1000084> PMID: 18551176
15. Sargeant TJ, Marti M, Caler E, Carlton JM, Simpson K, Speed TP, et al. Lineage-specific expansion of proteins exported to erythrocytes in malaria parasites. *Genome Biol*. 2006; 7(2):R12. <https://doi.org/10.1186/gb-2006-7-2-r12> PMID: 16507167
16. Boddey JA, Carvalho TG, Hodder AN, Sargeant TJ, Sleebs BE, Marapana D, et al. Role of plasmepsin V in export of diverse protein families from the *Plasmodium falciparum* exportome. *Traffic*. 2013; 14(5):532–50.
17. Hiller NL, Bhattacharjee S, van Ooij C, Liolios K, Harrison T, Lopez-Estrano C, et al. A host-targeting signal in virulence proteins reveals a secretome in malarial infection. *Science*. 2004; 306(5703):1934–7. <https://doi.org/10.1126/science.1102737> PMID: 15591203
18. Marti M, Good RT, Rug M, Knuepfer E, Cowman AF. Targeting malaria virulence and remodeling proteins to the host erythrocyte. *Science*. 2004; 306(5703):1930–3. <https://doi.org/10.1126/science.1102452> PMID: 15591202
19. Heiber A, Kruse F, Pick C, Gruring C, Flemming S, Oberli A, et al. Identification of new PNEPs indicates a substantial non-PEXEL exportome and underpins common features in *Plasmodium falciparum* protein export. *PLoS Pathog*. 2013; 9(8):e1003546. <https://doi.org/10.1371/journal.ppat.1003546> PMID: 23950716
20. Maier AG, Rug M, O'Neill MT, Brown M, Chakravorty S, Szestak T, et al. Exported proteins required for virulence and rigidity of *Plasmodium falciparum*-infected human erythrocytes. *Cell*. 2008; 134(1):48–61.
21. Jonsdottir TK, Gabriela M, Crabb BS, T FdK-W, Gilson PR. Defining the essential exportome of the malaria parasite. *Trends Parasitol*. 2021; 37(7):664–75. <https://doi.org/10.1016/j.pt.2021.04.009> PMID: 33985912
22. Nguiragool W, Bokhari AA, Pillai AD, Rayavara K, Sharma P, Turpin B, et al. Malaria parasite *clag3* genes determine channel-mediated nutrient uptake by infected red blood cells. *Cell*. 2011; 145(5):665–77.
23. Counihan NA, Chisholm SA, Bullen HE, Srivastava A, Sanders PR, Jonsdottir TK, et al. *Plasmodium falciparum* parasites deploy RhopH2 into the host erythrocyte to obtain nutrients, grow and replicate. *eLife*. 2017; 6:e23217. <https://doi.org/10.7554/eLife.23217> PMID: 28252383
24. Ito D, Schureck MA, Desai SA. An essential dual-function complex mediates erythrocyte invasion and channel-mediated nutrient uptake in malaria parasites. *eLife*. 2017; 6:e23485. <https://doi.org/10.7554/eLife.23485> PMID: 28221136
25. Sherling ES, Knuepfer E, Brzostowski JA, Miller LH, Blackman MJ, van Ooij C. The *Plasmodium falciparum* rhoptry protein RhopH3 plays essential roles in host cell invasion and nutrient uptake. *eLife*. 2017; 6:e23239.
26. Ahmad M, Manzella-Lapeira J, Saggù G, Ito D, Brzostowski JA, Desai SA. Live-cell FRET reveals that malaria nutrient channel proteins CLAG3 and RhopH2 remain associated throughout their tortuous trafficking. *mBio*. 2020; 11(5):e01354–20. <https://doi.org/10.1128/mBio.01354-20> PMID: 32900800
27. Pasternak M, Verhoef JMJ, Wong W, Triglia T, Mlodzianoski MJ, Geoghegan N, et al. RhopH2 and RhopH3 export enables assembly of the RhopH complex on *P. falciparum*-infected erythrocyte membranes. *Commun Biol*. 2022; 5(1):333.
28. Maier AG, Cooke BM, Cowman AF, Tilley L. Malaria parasite proteins that remodel the host erythrocyte. *Nat Rev Microbiol*. 2009; 7(5):341–54. <https://doi.org/10.1038/nrmicro2110> PMID: 19369950
29. Gomes PS, Bhardwaj J, Rivera-Correa J, Freire-De-Lima CG, Morrot A. Immune escape strategies of malaria parasites. *Front Microbiol*. 2016; 7:1617. <https://doi.org/10.3389/fmicb.2016.01617> PMID: 27799922
30. de Koning-Ward TF, Dixon MW, Tilley L, Gilson PR. *Plasmodium* species: master renovators of their host cells. *Nat Rev Microbiol*. 2016; 14(8):494–507.
31. Prommano P, Uthaipibull C, Wongsombat C, Kamchonwongpaisan S, Yuthavong Y, Knuepfer E, et al. Inducible knockdown of *Plasmodium* gene expression using the *glmS* ribozyme. *PLoS One*. 2013; 8(8):e73783.
32. Milani KJ, Schneider TG, Taraschi TF. Defining the morphology and mechanism of the hemoglobin transport pathway in *Plasmodium falciparum*-infected erythrocytes. *Eukaryot Cell*. 2015; 14(4):415–26.
33. Egan TJ, Combrinck JM, Egan J, Hearne GR, Marques HM, Ntenteni S, et al. Fate of haem iron in the malaria parasite *Plasmodium falciparum*. *Biochem J*. 2002; 365(Pt 2):343–7.

34. Dasaradhi PV, Korde R, Thompson JK, Tanwar C, Nag TC, Chauhan VS, et al. Food vacuole targeting and trafficking of falcipain-2, an important cysteine protease of human malaria parasite *Plasmodium falciparum*. *Mol Biochem Parasitol*. 2007; 156(1):12–23.
35. Subramanian S, Sijwali PS, Rosenthal PJ. Falcipain cysteine proteases require bipartite motifs for trafficking to the *Plasmodium falciparum* food vacuole. *J Biol Chem*. 2007; 282(34):24961–9.
36. Klemba M, Beatty W, Gluzman I, Goldberg DE. Trafficking of plasmepsin II to the food vacuole of the malaria parasite *Plasmodium falciparum*. *J Cell Biol*. 2004; 164(1):47–56.
37. Nasamu AS, Polino AJ, Istvan ES, Goldberg DE. Malaria parasite plasmepsins: More than just plain old degradative pepsins. *J Biol Chem*. 2020; 295(25):8425–41. <https://doi.org/10.1074/jbc.REV120.009309> PMID: 32366462
38. Lazarus MD, Schneider TG, Taraschi TF. A new model for hemoglobin ingestion and transport by the human malaria parasite *Plasmodium falciparum*. *J Cell Sci*. 2008; 121(11):1937–49.
39. Abu Bakar N, Klonis N, Hanssen E, Chan C, Tilley L. Digestive-vacuole genesis and endocytic processes in the early intraerythrocytic stages of *Plasmodium falciparum*. *J Cell Sci*. 2010; 123(Pt 3):441–50.
40. Krugliak M, Zhang J, Ginsburg H. Intraerythrocytic *Plasmodium falciparum* utilizes only a fraction of the amino acids derived from the digestion of host cell cytosol for the biosynthesis of its proteins. *Mol Biochem Parasitol*. 2002; 119(2):249–56.
41. Lew VL, Tiffert T, Ginsburg H. Excess hemoglobin digestion and the osmotic stability of *Plasmodium falciparum*-infected red blood cells. *Blood*. 2003; 101(10):4189–94.
42. Esposito A, Tiffert T, Mauritz JM, Schlaechter S, Bannister LH, Kaminski CF, et al. FRET imaging of hemoglobin concentration in *Plasmodium falciparum*-infected red cells. *PLoS One*. 2008; 3(11):e3780.
43. Lew VL, Macdonald L, Ginsburg H, Krugliak M, Tiffert T. Excess haemoglobin digestion by malaria parasites: a strategy to prevent premature host cell lysis. *Blood Cells Mol Dis*. 2004; 32(3):353–9. <https://doi.org/10.1016/j.bcmd.2004.01.006> PMID: 15121091
44. Goldberg DE, Slater AF, Beavis R, Chait B, Cerami A, Henderson GB. Hemoglobin degradation in the human malaria pathogen *Plasmodium falciparum*: a catabolic pathway initiated by a specific aspartic protease. *J Exp Med*. 1991; 173(4):961–9.
45. Dahl EL, Rosenthal PJ. Biosynthesis, localization, and processing of falcipain cysteine proteases of *Plasmodium falciparum*. *Mol Biochem Parasitol*. 2005; 139(2):205–12.
46. Banerjee R, Liu J, Beatty W, Pelosof L, Klemba M, Goldberg DE. Four plasmepsins are active in the *Plasmodium falciparum* food vacuole, including a protease with an active-site histidine. *Proc Natl Acad Sci U S A*. 2002; 99(2):990–5.
47. Sijwali PS, Rosenthal PJ. Gene disruption confirms a critical role for the cysteine protease falcipain-2 in hemoglobin hydrolysis by *Plasmodium falciparum*. *Proc Natl Acad Sci U S A*. 2004; 101(13):4384–9.
48. Omara-Opyene AL, Moura PA, Sulsona CR, Bonilla JA, Yowell CA, Fujioka H, et al. Genetic disruption of the *Plasmodium falciparum* digestive vacuole plasmepsins demonstrates their functional redundancy. *J Biol Chem*. 2004; 279(52):54088–96.
49. Shenai BR, Sijwali PS, Singh A, Rosenthal PJ. Characterization of native and recombinant falcipain-2, a principal trophozoite cysteine protease and essential hemoglobinase of *Plasmodium falciparum*. *J Biol Chem*. 2000; 275(37):29000–10.
50. Klonis N, Tan O, Jackson K, Goldberg D, Klemba M, Tilley L. Evaluation of pH during cytostomal endocytosis and vacuolar catabolism of haemoglobin in *Plasmodium falciparum*. *Biochem J*. 2007; 407(3):343–54.
51. Matz JM, Drepper B, Blum TB, van Genderen E, Burrell A, Martin P, et al. A lipocalin mediates unidirectional heme biomineralization in malaria parasites. *Proc Natl Acad Sci U S A*. 2020; 117(28):16546–56. <https://doi.org/10.1073/pnas.2001153117> PMID: 32601225
52. Makler MT, Hinrichs DJ. Measurement of the lactate dehydrogenase activity of *Plasmodium falciparum* as an assessment of parasitemia. *Am J Trop Med Hyg*. 1993; 48(2):205–10.
53. Persson KE, Lee CT, Marsh K, Beeson JG. Development and optimization of high-throughput methods to measure *Plasmodium falciparum*-specific growth inhibitory antibodies. *J Clin Microbiol*. 2006; 44(5):1665–73.
54. Sijwali PS, Koo J, Singh N, Rosenthal PJ. Gene disruptions demonstrate independent roles for the four falcipain cysteine proteases of *Plasmodium falciparum*. *Mol Biochem Parasitol*. 2006; 150(1):96–106.
55. Gabriela M, Matthews KM, Boshoven C, Kouskousis B, Jonsdottir TK, Bullen HE, et al. A revised mechanism for how *Plasmodium falciparum* recruits and exports proteins into its erythrocytic host cell. *PLoS Pathog*. 2022; 18(2):e1009977.

56. Egan TJ. Recent advances in understanding the mechanism of hemozoin (malaria pigment) formation. *J Inorg Biochem.* 2008; 102(5–6):1288–99. <https://doi.org/10.1016/j.jinorgbio.2007.12.004> PMID: 18226838
57. Francis SE, Banerjee R, Goldberg DE. Biosynthesis and maturation of the malaria aspartic hemoglobinases plasmepsins I and II. *J Biol Chem.* 1997; 272(23):14961–8. <https://doi.org/10.1074/jbc.272.23.14961> PMID: 9169469
58. Banerjee R, Francis SE, Goldberg DE. Food vacuole plasmepsins are processed at a conserved site by an acidic convertase activity in *Plasmodium falciparum*. *Mol Biochem Parasitol.* 2003; 129(2):157–65.
59. Azevedo MF, Nie CQ, Elsworth B, Charnaud SC, Sanders PR, Crabb BS, et al. *Plasmodium falciparum* transfected with ultra bright NanoLuc luciferase offers high sensitivity detection for the screening of growth and cellular trafficking inhibitors. *PLoS One.* 2014; 9(11):e112571. <https://doi.org/10.1371/journal.pone.0112571> PMID: 25392998
60. Eilers M, Schatz G. Binding of a specific ligand inhibits import of a purified precursor protein into mitochondria. *Nature.* 1986; 322(6076):228–32. <https://doi.org/10.1038/322228a0> PMID: 3016548
61. Gehde N, Hinrichs C, Montilla I, Charpian S, Lingelbach K, Przyborski JM. Protein unfolding is an essential requirement for transport across the parasitophorous vacuolar membrane of *Plasmodium falciparum*. *Mol Microbiol.* 2009; 71(3):613–28.
62. Mesen-Ramirez P, Reinsch F, Blancke Soares A, Bergmann B, Ullrich AK, Tenzer S, et al. Stable translocation intermediates jam global protein export in *Plasmodium falciparum* parasites and link the PTEX component EXP2 with translocation activity. *PLoS Pathog.* 2016; 12(5):e1005618. <https://doi.org/10.1371/journal.ppat.1005618> PMID: 27168322
63. Charnaud SC, Jonsdottir TK, Sanders PR, Bullen HE, Dickerman BK, Kouskousis B, et al. Spatial organization of protein export in malaria parasite blood stages. *Traffic.* 2018; 19(8):605–23. <https://doi.org/10.1111/tra.12577> PMID: 29696751
64. Benting J, Mattei D, Lingelbach K. Brefeldin A inhibits transport of the glycophorin-binding protein from *Plasmodium falciparum* into the host erythrocyte. *Biochem J.* 1994; 300 (Pt 3):821–6.
65. Crary JL, Haldar K. Brefeldin A inhibits protein secretion and parasite maturation in the ring stage of *Plasmodium falciparum*. *Mol Biochem Parasitol.* 1992; 53(1–2):185–92.
66. Bullen HE, Sanders PR, Dans MG, Jonsdottir TK, Riglar DT, Looker O, et al. The *Plasmodium falciparum* parasitophorous vacuole protein P113 interacts with the parasite protein export machinery and maintains normal vacuole architecture. *Mol Microbiol.* 2022; 117(5):1245–62.
67. Jackson KE, Spielmann T, Hanssen E, Adisa A, Separovic F, Dixon MW, et al. Selective permeabilization of the host cell membrane of *Plasmodium falciparum*-infected red blood cells with streptolysin O and equinatoxin II. *Biochem J.* 2007; 403(1):167–75. <https://doi.org/10.1042/BJ20061725> PMID: 17155936
68. Perkins M. Stage-dependent processing and localization of a *Plasmodium falciparum* protein of 130,000 molecular weight. *Exp Parasitol.* 1988; 65(1):61–8.
69. Blackman MJ. Malarial proteases and host cell egress: an 'emerging' cascade. *Cell Microbiol.* 2008; 10 (10):1925–34. <https://doi.org/10.1111/j.1462-5822.2008.01176.x> PMID: 18503638
70. Francis SE, Sullivan DJ Jr, Goldberg DE. Hemoglobin metabolism in the malaria parasite *Plasmodium falciparum*. *Annu Rev Microbiol.* 1997; 51:97–123.
71. Gupta P, Pandey R, Thakur V, Parveen S, Kaur I, Panda A, et al. Heme Detoxification Protein (PfHDP) is essential for the hemoglobin uptake and metabolism in *Plasmodium falciparum*. *FASEB BioAdvances.* 2022; 00:1–13. <https://doi.org/10.1096/fba.2022-00021> PMID: 36238365
72. Mesen-Ramirez P, Bergmann B, Tran TT, Garten M, Stacker J, Naranjo-Prado I, et al. EXP1 is critical for nutrient uptake across the parasitophorous vacuole membrane of malaria parasites. *PLoS Biol.* 2019; 17(9):e3000473. <https://doi.org/10.1371/journal.pbio.3000473> PMID: 31568532
73. Drew ME, Banerjee R, Uffman EW, Gilbertson S, Rosenthal PJ, Goldberg DE. *Plasmodium* food vacuole plasmepsins are activated by falcipains. *J Biol Chem.* 2008; 283(19):12870–6.
74. Gruring C, Heiber A, Kruse F, Flemming S, Franci G, Colombo SF, et al. Uncovering common principles in protein export of malaria parasites. *Cell Host Microbe.* 2012; 12(5):717–29. <https://doi.org/10.1016/j.chom.2012.09.010> PMID: 23159060
75. Matthews KM, Pitman EL, de Koning-Ward TF. Illuminating how malaria parasites export proteins into host erythrocytes. *Cell Microbiol.* 2019; 21(4):e13009. <https://doi.org/10.1111/cmi.13009> PMID: 30656810
76. Egea PF, Stroud RM. Lateral opening of a translocon upon entry of protein suggests the mechanism of insertion into membranes. *Proc Natl Acad Sci U S A.* 2010; 107(40):17182–7. <https://doi.org/10.1073/pnas.1012556107> PMID: 20855604

77. Schureck MA, Darling JE, Merk A, Shao J, Daggupati G, Srinivasan P, et al. Malaria parasites use a soluble RhopH complex for erythrocyte invasion and an integral form for nutrient uptake. *Elife*. 2021; 10: e65282. <https://doi.org/10.7554/elife.65282> PMID: 33393463
78. Riglar DT, Rogers KL, Hanssen E, Turnbull L, Bullen HE, Charnaud SC, et al. Spatial association with PTEX complexes defines regions for effector export into *Plasmodium falciparum*-infected erythrocytes. *Nat Commun*. 2013; 4:1415. <https://doi.org/10.1038/ncomms2449> PMID: 23361006
79. Birnbaum J, Scharf S, Schmidt S, Jonscher E, Hoeijmakers WAM, Flemming S, et al. A Kelch13-defined endocytosis pathway mediates artemisinin resistance in malaria parasites. *Science*. 2020; 367 (6473):51–9. <https://doi.org/10.1126/science.aax4735> PMID: 31896710
80. Adjalley S, Lee MCS. CRISPR/Cas9 Editing of the *Plasmodium falciparum* Genome. *Methods Mol Biol*. 2022; 2470:221–39. [https://doi.org/10.1007/978-1-0716-2189-9\\_17](https://doi.org/10.1007/978-1-0716-2189-9_17) PMID: 35881349
81. Ribeiro JM, Garriga M, Potchen N, Crater AK, Gupta A, Ito D, et al. Guide RNA selection for CRISPR-Cas9 transfections in *Plasmodium falciparum*. *Int J Parasitol*. 2018; 48(11):825–32.
82. Trager W, Jensen JB. Human malaria parasites in continuous culture. *Science*. 1976; 193(4254):673–5. <https://doi.org/10.1126/science.781840> PMID: 781840
83. Boyle MJ, Richards JS, Gilson PR, Chai W, Beeson JG. Interactions with heparin-like molecules during erythrocyte invasion by *Plasmodium falciparum* merozoites. *Blood*. 2010; 115(22):4559–68.
84. Ressurreicao M, Thomas JA, Nofal SD, Flueck C, Moon RW, Baker DA, et al. Use of a highly specific kinase inhibitor for rapid, simple and precise synchronization of *Plasmodium falciparum* and *Plasmodium knowlesi* asexual blood-stage parasites. *PLoS One*. 2020; 15(7):e0235798. <https://doi.org/10.1371/journal.pone.0235798> PMID: 32673324
85. Jonsdottir TK, Counihan NA, Modak JK, Kouskousis B, Sanders PR, Gabriela M, et al. Characterisation of complexes formed by parasite proteins exported into the host cell compartment of *Plasmodium falciparum* infected red blood cells. *Cellular Microbiology*. 2021; 23(8):e13332.
86. Tonkin CJ, van Dooren GG, Spurck TP, Struck NS, Good RT, Handman E, et al. Localization of organelar proteins in *Plasmodium falciparum* using a novel set of transfection vectors and a new immunofluorescence fixation method. *Mol Biochem Parasitol*. 2004; 137(1):13–21.
87. Sanders PR, Dickerman BK, Charnaud SC, Ramsland PA, Crabb BS, Gilson PR. The N-terminus of EXP2 forms the membrane-associated pore of the protein exporting translocon PTEX in *Plasmodium falciparum*. *J Biochem*. 2019; 165(3):239–48.
88. Cobbold SA, Chua HH, Nijagal B, Creek DJ, Ralph SA, McConville MJ. Metabolic dysregulation induced in *Plasmodium falciparum* by dihydroartemisinin and other front-line antimalarial drugs. *J Infect Dis*. 2016; 213(2):276–86.
89. Clasquin MF, Melamud E, Rabinowitz JD. LC-MS data processing with MAVEN: a metabolomic analysis and visualization engine. *Curr Protoc Bioinformatics*. 2012; Chapter 14:Unit14 1. <https://doi.org/10.1002/0471250953.bi1411s37> PMID: 22389014